

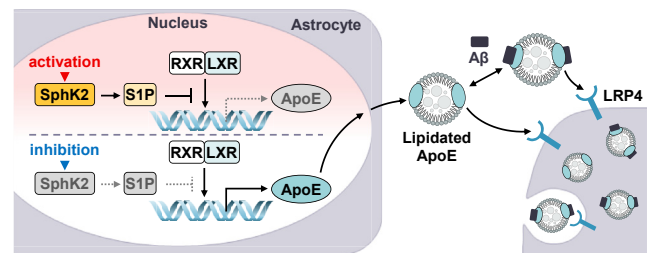
# Nuclear SphK2/S1P signaling is a key regulator of ApoE production and A $\beta$ uptake in astrocytes

Masato Komai<sup>1,2</sup>, Yuka Noda<sup>1</sup>, Atsuya Ikeda<sup>1</sup>, Nanaka Kaneshiro<sup>1</sup> , Yuji Kamikubo<sup>3</sup> , Takashi Sakurai<sup>3</sup> , Takashi Uehara<sup>1</sup> , and Nobumasa Takasugi<sup>1,3,\*</sup> 

<sup>1</sup>Department of Medicinal Pharmacology, Graduate School of Medicine, Dentistry and Pharmaceutical Sciences, Okayama University, Kita, Okayama, Japan; <sup>2</sup>Research Fellow of Japan Society for the Promotion of Science, Chiyoda, Tokyo, Japan; <sup>3</sup>Department of Cellular and Molecular Pharmacology, Juntendo University Graduate School of Medicine, Bunkyo, Tokyo, Japan

**Abstract** The link between changes in astrocyte function and the pathological progression of Alzheimer's disease (AD) has attracted considerable attention. Interestingly, activated astrocytes in AD show abnormalities in their lipid content and metabolism. In particular, the expression of apolipoprotein E (ApoE), a lipid transporter, is decreased. Because ApoE has anti-inflammatory and amyloid  $\beta$  (A $\beta$ )-metabolizing effects, the nuclear receptors, retinoid X receptor (RXR) and LXR, which are involved in ApoE expression, are considered promising therapeutic targets for AD. However, the therapeutic effects of agents targeting these receptors are limited or vary considerably among groups, indicating the involvement of an unknown pathological factor that modifies astrocyte and ApoE function. Here, we focused on the signaling lipid, sphingosine-1-phosphate (S1P), which is mainly produced by sphingosine kinase 2 (SphK2) in the brain. Using astrocyte models, we found that upregulation of SphK2/S1P signaling suppressed ApoE induction by both RXR and LXR agonists. We also found that SphK2 activation reduced RXR binding to the *APOE* promoter region in the nucleus, suggesting the nuclear function of SphK2/S1P. Intriguingly, suppression of SphK2 activity by RNA knockdown or specific inhibitors upregulated lipidated ApoE induction. Furthermore, the induced ApoE facilitates A $\beta$  uptake in astrocytes. Together with our previous findings that SphK2 activity is upregulated in AD brain and promotes A $\beta$  production in neurons, these results indicate that SphK2/S1P signaling is a promising multifunctional therapeutic target for AD that can modulate astrocyte function by stabilizing the effects of RXR and LXR agonists, and simultaneously regulate neuronal pathogenesis.

**Supplementary key words** alzheimer's disease • apolipoproteins • nuclear receptors/RXR • transcription • sphingosine phosphate • astrocytes • amyloid  $\beta$  • sphingosine kinase 2 • low-density lipoprotein receptor-related protein 4



Alzheimer's disease (AD) is a neurodegenerative disease characterized by extracellular accumulation of senile plaques composed mainly of amyloid  $\beta$  (A $\beta$ ), and intracellular neurofibrillary tangles composed of highly phosphorylated tau. A $\beta$  accumulates in the brain prior to tau protein, and the imbalance between A $\beta$  production and clearance is considered to be a cause of AD (1). Thus, A $\beta$ -targeted therapeutics have been developed, and A $\beta$  antibodies have received Food and Drug Administration approval for the treatment of AD. However, their efficacy in improving cognitive function is limited (2, 3), suggesting the need for comprehensive regulation of the brain environment, including A $\beta$ .

Recently, neuroinflammation has attracted attention as the third hallmark of AD pathology (4). Neuroinflammation is characterized by the activation of glial cells, such as microglia and astrocytes, and impairs brain network function through the abnormal production of inflammatory cytokines. Notably, astrocyte activity is an executing factor (5). Astrocytes are the most abundant cell type in the brain and are responsible for maintaining lipid homeostasis (6). Astrocyte activation leading to a chronic inflammatory response has been proposed as a mechanism linking A $\beta$  accumulation and

\*For correspondence: Nobumasa Takasugi, [ntakasu@okayama-u.ac.jp](mailto:ntakasu@okayama-u.ac.jp).

tau pathology (7) and is considered to be one of the important pathological processes in AD. In addition, reactive astrocytes induced by microglial activation induce cell toxicity via the secretion of saturated lipids (5, 8). Therefore, alterations in astrocyte function and lipid regulatory mechanisms are highly relevant to the pathophysiology of AD.

Interestingly, apolipoprotein E (ApoE), a major mediator of lipid transport in the brain, is down-regulated in astrocytes in AD (9, 10), suggesting the imbalance of lipid metabolism. Because ApoE is mainly produced in astrocytes and has anti-inflammatory and A $\beta$ -metabolizing effects, its induction is a promising therapeutic target for AD. ApoE expression is coordinately regulated by the ligand-activated nuclear receptors, retinoid X receptor (RXR) and LXR. Indeed, the administration of RXR or LXR agonists reduces A $\beta$  aggregation and restores cognitive function in AD mouse model (11, 12). However, the therapeutic effects of RXR agonists, especially bexarotene, varied widely in follow-up studies (13–16), suggesting that there is an unknown pathological factor causing this variation, and that the regulatory mechanism of RXR-ApoE needs to be elucidated to develop effective AD treatments.

In this study, we focused on sphingosine-1-phosphate (SIP), a signaling lipid, which we have previously shown to be involved in A $\beta$  production in neurons (17). In brain, SIP is mainly generated by phosphorylation of sphingosine by sphingosine kinase 2 (SphK2). Because the deficiency of SGPL1, an SIP-degrading enzyme, leads to induction of astrogliosis (18), elevated levels of SIP are considered an important activator of astrocyte. Interestingly, A $\beta$  aggregation in AD model mice was reduced upon SphK2 KO (19), predicting a link between SphK2 activity and the disease state. Furthermore, because SIP is associated with transcriptional regulation to alter cellular function (20), we analyzed the relationship between SphK2/SIP signaling and ApoE using several astrocyte models.

## MATERIAL AND METHODS

### Reagents and antibodies

T0901317, bexarotene, ABC294640, SLM6031434, and FTY720 were purchased from Cayman Chemical (Ann Arbor, MI). Trichostatin A (#HY-15144) was purchased from MedChemExpress (Monmouth Junction, NJ). Synthetic A $\beta$ <sub>1-42</sub> peptide (Peptide Institute, Osaka, Japan) was solubilized in hexafluoro-2-propanol at a concentration of 1 mg/ml to prevent self-aggregation. For immunoblotting and immunostaining, antibodies against human A $\beta$  N terminal (clone 82E1; Immuno-Biological Laboratories, Gunma, Japan), ATP binding cassette transporter A1 (ABCA1) (clone HJ1; Abnova, Taipei, Taiwan), ApoE (#AB947; Merck Millipore, Burlington, MA),  $\alpha$ -tubulin (clone 10G10; Fujifilm Wako, Osaka, Japan),  $\beta$ -actin (#5125; Cell Signaling Technology, Danvers, MA),

GAPDH (#2118; Cell Signaling Technology), glial fibrillary acidic protein (GFAP) (#GTX10871; GeneTex, Irvine, CA), Lamin A/C (#10298-1-AP; Proteintech, Rosemont, IL), LXR $\alpha$ / $\beta$  (#sc-377260; Santa Cruz Biotechnology, Dallas, TX), nuclear factor- $\kappa$ B (NF- $\kappa$ B) p65 (#8242; Cell Signaling Technology), RXR $\alpha$  (#sc-515929; Santa Cruz Biotechnology), SphK2 (#17096-1-AP; Proteintech), and 6His (#66005-1-Ig; Proteintech) were purchased from the indicated vendors.

### Plasmids

pcDNA3.1-SphK2-V5-6His: The expression vector for human SphK2 conjugated with V5 and 6His tag in pcDNA3.1 vector was previously described (17).

pCAGGS-BLRP-hRXR $\alpha$ -IRES-BirA: pCAGGS-BLRP-IRES-BirA vector was purchased from RIKEN BRC (Ibaraki, Japan). The sequence of human RXR $\alpha$  was amplified from complementary DNA (cDNA) from U87 cells and inserted into pCAGGS-BLRP-IRES-BirA digested with NotI to express hRXR $\alpha$  N terminally fused to the biotin ligase recognition peptide (BLRP) sequence. To concatenate vector with DNA fragment, In-Fusion cloning system (TaKaRa Bio, Shiga, Japan) was used.

pFN21AA0816-LRP4-V5-6His: To express low-density lipoprotein receptor-related protein 4 (LRP4) fused with V5-6His tag at the C terminus, LRP4-Halo expression plasmid, pFN21AA0816, was purchased from Kazusa DNA Research Institute (Chiba, Japan). The vector was digested with NheI and AsiSI to eliminate the HaloTag sequence and replace the multi cloning site amplified from the pEBMulti-Hyg vector (Fujifilm Wako). The constructed vector was further cut with PmeI to insert the V5 and 6His tag sequence from the pcDNA3.1 vector. To concatenate vector with DNA fragment, NEBuilder HiFi DNA Assembly system (New England Biolabs, Ipswich, MA) was used.

pAAV2-CMV-SphK2: pAAV2-CMV vector was purchased from TaKaRa Bio. The DNA sequence encoding human SphK2-V5-6His was subcloned into the SpeI-digested pAAV2-CMV vector.

pAAV2-GfaABC<sub>1</sub>D-SphK2: The astrocyte-specific promoter, the GfaABC<sub>1</sub>D sequence (21) was synthesized by Thermo Fisher Scientific (Waltham, MA). pAAV2-CMV vector was digested with HindIII and EcoRI to remove the cytomegalovirus (CMV) promoter sequence and replace it with the GfaABC<sub>1</sub>D sequence. The DNA sequence encoding human SphK2 V5-6His tag-conjugate was subcloned into pAAV2-GfaABC<sub>1</sub>D vector digested with SpeI.

All constructed plasmids and inserted sequences were verified by Sanger sequencing (Azenta Life Sciences, Burlington, MA).

### Cell culture

Human astrocytoma U87 MG (U87) and human embryonic kidney (HEK) 293T cells were cultured in DMEM supplemented with 10% (v/v) heat-inactivated FBS and 1% penicillin/streptomycin at 37°C in a humidified atmosphere of CO<sub>2</sub>/95% air.

Human primary astrocytes (#CC-2565) derived from normal fetuses at 19 weeks of gestation were purchased from Lonza (Basel, Switzerland). Astrocytes were cultured in 1 $\times$ ABM™ Basal Medium (#CC-3187; Lonza) containing 1 $\times$ AGM™ SingleQuots™ Supplement Pack (#CC-4123; Lonza) [FBS, L-glutamine, GA-1000, ascorbic acid, hEGF, and insulin].

## Establishment of stable cell line

The pcDNA3.1-SphK2-V5-6His vector was introduced into U87 cells using Lipofectamine® 2000 (Thermo Fisher Scientific). Cells were selected with 500 µg/ml of Geneticin (G418).

## Immunoblotting

To detect ApoE and ABCA1, cells were preincubated with LXR or RXR agonist for 48 h in serum-free medium containing 1% penicillin/streptomycin and 0.1% BSA. To examine the effect of SphK2 on ApoE expression, cells were cotreated with SphK2 specific inhibitor or FTY720, and LXR or RXR agonist for 48 h.

Cell medium was mixed with 0.1 µM PMSF. After centrifugation (800 g, 4°C, 10 min), the supernatant was collected.

Cells were washed with ice-cold PBS and lysed with RIPA buffer [50 mM Tris-HCl (pH 7.5), 150 mM NaCl, 0.1% SDS, 1% Triton X-100, and 1% sodium deoxycholate containing protease inhibitor cocktail (Roche, Basel, Switzerland)] for 10 min on ice.

After BCA protein assay, the samples were boiled in SDS sample buffer [62.5 mM Tris-HCl (pH 6.8), 5% 2-mercaptoethanol, 2% SDS, and 10% glycerol], and separated by SDS-PAGE. The separated proteins were transferred to a 0.4 µm PVDF membrane. This membrane was blocked with nonfat milk in Tris-buffered saline containing 0.1% Tween-20 and incubated with appropriate primary antibodies at 4°C overnight. Then, HRP-conjugated secondary antibodies were applied to the membrane at room temperature for 1 h. Protein bands were visualized by the enhanced chemiluminescence system using the ChemiDoc™ MP Imaging System (Bio-Rad Laboratories, Hercules, CA). For the densitometric analysis, Image Lab software (Bio-Rad Laboratories; <https://www.bio-rad.com/en-jp/product/image-lab-software?ID=KRE6P5E8Z>) was used.

To detect Aβ<sub>1-42</sub>, Tris-Tricine SDS-PAGE was employed. The separated proteins were transferred to a 0.2 µm PVDF membrane (#BSP0161; PALL Life Science, Port Washington, NY). This membrane was boiled in PBS to expose the Aβ<sub>1-42</sub> antigenic site before blocking with nonfat milk.

The same amount of protein was applied to each sample. The densitometric intensity of each blot was measured and normalized by the loading control indicated in the figure legends and used for statistical analysis.

## RT-PCR

Cells were washed with ice-cold PBS. Total RNA from U87 cells was extracted by the phenol-chloroform method using TRI reagent (#TR118; Molecular Research Center, Cincinnati, OH) and chloroform. ReverTra Ace (#TRT-101; TOYOBO, Osaka, Japan) was used to synthesize cDNA according to the manufacturer's instructions. The PCR was performed with Expand High Fidelity<sup>PLUS</sup> PCR System (Roche) under the following conditions. PCR products were separated on 2% agarose gels. DNA bands were visualized with 0.5 ng/ml ethidium bromide using the Gel Doc™ EZ System (Bio-Rad Laboratories). For analysis, Image Lab software was used, and the densitometric intensity was normalized by the level of actin beta (*ACTB*).

## Primer sequences

Name	Primer Sequences
<i>APOE</i>	Forward 5'- TGT TGG TCC CAT TGC TGA CAG GAT -3'
	Reverse 5'- TGG TGT TTA CCT CGT TGC GGT ACT -3'
<i>ABCA1</i>	Forward 5'- GCA CTG AGG AAG ATG CTG AAA -3'
	Reverse 5'- AGT TCC TGG AAG GTC TTG TTC AC -3'
<i>ACTB</i>	Forward 5'- CCT GAC GGC CAG GTC ATC -3'
	Reverse 5'- GGA CTC GTC ATA CTC CTG -3'

## Reverse transcription-quantitative PCR

Cells were washed with ice-cold PBS. Total RNA from U87 cells was extracted by the phenol-chloroform method using TRI reagent and chloroform. ReverTra Ace qPCR RT Master Mix (#FSQ-201; TOYOBO) was used to synthesize cDNA according to the manufacturer's instructions. qPCR was performed using KOD SYBR qPCR Mix (#QKD-201; TOYOBO) under the following conditions: 98°C for 2 min, followed by 40 cycles of 98°C for 10 s, 60°C for 10 s, and 68°C for 30 s using CFX Duet (Bio-Rad Laboratories). All qPCRs amplified single products, as confirmed by the melting curve and electrophoresis using 2% agarose gels with 0.5 ng/ml ethidium bromide. The following primer sets were used. The 2<sup>-ΔΔCt</sup> relative quantification method, using *ACTB* for normalization, was used to estimate target gene expression. The fold-change was calculated relative to the mRNA expression levels in the control samples.

## Primer sequences

Name	Primer Sequences
<i>APOE</i>	Forward 5'- GAG CAA GCG GTG GAG ACA G -3'
	Reverse 5'- CAT CAG CGC CCT CAG TTC C -3'
<i>ABCA1</i>	Forward 5'- GCA AGG CTA CCA GTT ACA TTT G -3'
	Reverse 5'- GTC AGA AAC ATC ACC TCC TG -3'
<i>APOJ</i>	Forward 5'- TCT TCT TTC CCA AGT CCC GC -3'
	Reverse 5'- TCA TCG TCG CCT TCT CGT ATG -3'
<i>IL6</i>	Forward 5'- ACT CAC CTC TTC AGA ACG AAT TG -3'
	Reverse 5'- CCA TCT TTG GAA GGT TCA GGT TG -3'
<i>IL1β</i>	Forward 5'- ATG ATG GCT TAT TAC AGT GGC AA -3'
	Reverse 5'- GTC GGA GAT TCG TAG CTG GA -3'
<i>ACTB</i>	Forward 5'- TCA CCC ACA CTG TGC CCA TCT ACG A -3'
	Reverse 5'- CAG CGG AAC CGC TCA TTG CCA CTG G -3'

## In vitro SphK2 activity assay

SphK2 activity assay was performed as previously described (17). Briefly, cells were washed with ice-cold PBS and lysed by freeze-thaw cycle in 50 mM HEPES (pH 7.4), 10 mM KCl, 15 mM MgCl<sub>2</sub>, 20% glycerol, 2 mM Na<sub>3</sub>VO<sub>4</sub>, 2 mM DTT, 10 mM NaF, 1 mM deoxyypyridoxine, and EDTA-free complete protease inhibitor (Roche). Samples were centrifuged at 20,600 g for 10 min and the supernatants were collected. The lysates and

7-nitro-2,1,3-benzoxadiazole (NBD)-Sphingosine (Cayman Chemical) were mixed in the reaction buffer [50 mM HEPES (pH 7.4), 15 mM MgCl<sub>2</sub>, 0.5 M KCl, 10% glycerol, and 2 mM ATP] and incubated at 37°C for 30 min. The reactions were stopped by the addition of an equal volume of 1 M potassium phosphate (pH 8.5), followed by the addition of 2.5-times chloroform/methanol (2:1), and then centrifuged at 20,600 *g* for 1 min. The alkaline aqueous phase containing NBD-SIP, but not NBD-Sphingosine, was collected. After the aqueous phase combining with an equal volume of dimethylformamide, the fluorescence intensity was measured using the GloMax-Multi Detection System (Promega, Madison, WI).

### RNA interference knockdown

For SphK2 knockdown, the following siRNA targeting the SphK2 untranslated region (2639–2661) was purchased from Sigma-Aldrich (St. Louis, MO); (sense) ACA UUA GUG CAA AUC CUA GCG, (antisense) CUA GGA UUU GCA CUA AUG UUC. This siRNA sequence was introduced into U87 cells with Lipofectamine® 2000 or Lipofectamine™ RNAiMAX (Thermo Fisher Scientific).

For ApoE knockdown, the siRNA targeting ApoE was purchased from Sigma-Aldrich (#SASI\_Hs01\_00154592). This siRNA sequence was introduced into U87 cells with Lipofectamine™ RNAiMAX.

### Establishment of adeno-associated virus (AAV) vector and transduction

AAV was produced using the AAVpro Helper Free system (#6230; TaKaRa Bio) according to the manufacturer's protocol. AAV particles were produced in HEK293T cells by cotransfection with pAAV2-CMV-SphK2, pRC2-mi342, and pHelper vector. Following day, the medium was changed to DMEM containing 2% FBS and 1% penicillin/streptomycin. At 48 h post transfection, AAV was extracted from AAV-producing HEK293T cells using AAV extraction solution (#6235; TaKaRa Bio). The final titers used in the experiments were  $1.88 \times 10^8$  copies/ml. Titers were determined by quantitative PCR using AAVpro® Titration Kit (for Real Time PCR) Ver.2 (#6233; TaKaRa Bio).

AAVs were transduced into human primary astrocytes for 48 h. Cell medium was mixed with 0.1 μM PMSF. After centrifugation (800 *g*, 4°C, 10 min), the supernatant was collected. Cells were washed with ice-cold PBS and lysed with RIPA buffer for 10 min on ice.

### Hippocampal slice culture

All animal experiments were performed in strict accordance with the institutional guidelines for animal experiments of Okayama University. The protocol was approved by the Animal Experimentation Committee of Okayama University (approval number: OKU-2022622). All animals were maintained in an environment at 24°C with a 12 h light/dark cycle, with water and food freely available.

C57BL/6J mice (postnatal days 7–10) were obtained from CLEA Japan (Tokyo, Japan). Hippocampal slice culture was performed as previously described (22, 23). For slice culture, adult mice were euthanized by decapitation after pentobarbital administration. Pups were euthanized by decapitation under hypothermic anesthesia. Mouse brains were sectioned into 400 μm thick slices using a tissue chopper [McIlwain] with a cutting blade. The hippocampal slices were dissected out and incubated at 4°C for 60 min in incubation medium

containing minimum essential medium, 9 mM Tris, 22.9 mM HEPES, and 63.1 mM glucose supplemented with penicillin/streptomycin. The slices were placed on Omnipore® membrane filters (#JHWP02500; Merck Millipore) on the doughnut plate (Hazai-Ya, Tokyo, Japan) in a solution containing 50% minimum essential medium, 25% HBSS, 25% horse serum (#H1138; Sigma-Aldrich), 6.6 mM Tris, 16.9 mM HEPES, 4 mM NaHCO<sub>3</sub>, and 29.8 mM glucose. The prepared slices were maintained at 37°C with 5% CO<sub>2</sub>/95% air. The culture medium was replaced twice per week.

For ApoE induction, the serum concentration was gradually decreased from 4 to 6 days in vitro (DIV) and replaced with B-27 (#17504044; Thermo Fisher Scientific) -supplemented Neurobasal-A medium (#10888022; Thermo Fisher Scientific).

### Establishment of astrocyte-specific AAV vector and transduction

AAV was produced using the AAVpro Helper Free system according to the manufacturer's protocol. AAV particles were produced in HEK293T cells by cotransfection with pAAV2-GfaABC<sub>1</sub>D-SphK2, pRC2-mi342, and pHelper vector. Following day, the medium was changed to DMEM containing 1% penicillin/streptomycin. At 48 h post transfection, AAV was extracted from AAV-producing HEK293T cells using AAV extraction solution. The final titers used in the experiments were  $2.19 \times 10^8$  copies/ml. Titers were determined by quantitative PCR using AAVpro® Titration Kit (for Real Time PCR) Ver.2. AAVs were transduced into hippocampal slices at DIV1.

### Immunostaining for cultured hippocampal slice

For immunostaining, the cultured slices were fixed with 4% paraformaldehyde in PBS at 4°C for 1 h. The fixed slices were washed with PBS and permeabilized with PBS containing 1% Triton X-100 and 5% horse serum at room temperature for 1 h. Slices were incubated with primary antibodies against GFAP (1:500) and 6His (1:200) at 4°C for 48 h. Slices were washed three times with PBS and incubated with secondary antibodies conjugated with Alexa Fluor 488 or 594 (1:500) at 4°C overnight. Slices were washed three times with PBS and then treated with VECTASHIELD Vibrance Antifade Mounting Medium with 4',6-diamidino-2-phenylindole (DAPI) (#H-1800; Vector Laboratories, Newark, CA). Images were obtained using BZ-X800 (Keyence, Osaka, Japan).

### Immunoblotting for cultured hippocampal slice

To detect ApoE, slices were preincubated with RXR agonist for 48 or 96 h in serum-free condition.

The medium was mixed with 0.1 μM PMSF. After centrifugation (800 *g*, 4°C, 10 min), the supernatant was collected.

Cultured hippocampal slices were washed with ice-cold PBS and lysed with RIPA buffer [25 mM Tris-HCl (pH 7.5), 137 mM NaCl, 3 mM KCl, 0.1% SDS, 1% NP-40, and 0.5% sodium deoxycholate containing protease inhibitor cocktail] (24). After BCA protein assay, the samples were boiled in SDS sample buffer and separated by SDS-PAGE.

### Nuclear extraction

Nuclear extraction was performed using Nuclear Extract Kit (#40010; Active Motif, Carlsbad, CA). The cell medium was removed, and the cells were collected in phosphatase/PBS using a cell lifter. After centrifugation (200 *g*, 4°C, 5 min), the

cell pellet was suspended in hypotonic buffer and detergent. This suspension was centrifuged (14,000 g, 4°C, 30 s) and the supernatant was collected as the cytoplasmic fraction. The pellet was resuspended in lysis buffer and detergent. After centrifugation (14,000 g, 4°C, 10 min), the supernatant was collected as the nuclear fraction.

### Chromatin immunoprecipitation (ChIP)

U87 cells were transfected with pCAGGS-BLRP-hRXR $\alpha$ -IRES-BirA using Lipofectamine® 3000 (Thermo Fisher Scientific). The medium was changed to serum-free medium containing 1% penicillin/streptomycin, 0.1% BSA, and 50  $\mu$ g/ml D-biotin 24 h after the transfection. Following day, the cells were treated with bexarotene for 3 h.

DNA and protein were cross-linked with 1% formaldehyde at room temperature for 10 min. Then, 0.15 M glycine was added to quench cross-linking. Fixed cells were washed with the buffer containing PBS and 2% FBS and lysed with SDS lysis buffer [50 mM Tris-HCl (pH 8.0), 10 mM EDTA (pH 8.0), and 1% SDS containing protease inhibitor cocktail]. The cells were then sonicated with 30 s pulses (output: 6) for 5 cycles, with a 1 min interval using a sonicator (#VP-5s; TAITEC, Saitama, Japan) and centrifuged (20,600 g, 8°C, 10 min). The supernatant was diluted in ChIP dilution buffer [50 mM Tris-HCl (pH 8.0), 167 mM NaCl, 1.1% Triton X-100, and 0.11% sodium deoxycholate containing protease inhibitor cocktail], and one-tenth samples were collected as input samples.

For the pull-down, NeutrAvidin™ Agarose (#29220; Thermo Fisher Scientific) was washed twice with RIPA buffer for ChIP [50 mM Tris-HCl (pH 8.0), 150 mM NaCl, 1 mM EDTA, 1% Triton X-100, 0.1% SDS, and 0.1% sodium deoxycholate], and resuspended with salmon sperm DNA in RIPA buffer to give a 50% slurry. The beads were mixed with the ChIP sample and rotated at 4°C overnight. The beads were then washed with RIPA buffer containing 150 mM or 500 mM NaCl, LiCl wash buffer [10 mM Tris-HCl (pH 8.0), 0.25 M LiCl, 1 mM EDTA, 0.5% NP-40, and 0.5% sodium deoxycholate], and Tris-EDTA buffer. After washing, the beads were eluted with ChIP elution buffer [10 mM Tris-HCl (pH 8.0), 300 mM NaCl, 5 mM EDTA, and 0.5% SDS]. DNA-protein crosslinks were reversed at 65°C for 4 h, then treated with RNase and proteinase K at 37°C for 30 min and at 55°C for 1 h, respectively. DNA was purified by phenol/chloroform extraction and eluted with Tris-EDTA buffer. Finally, the target DNA was amplified by PCR. The following primers were designed against the LXR response element region in *APOE* promoter (25). The sequence specificity was confirmed by GGGenome (<https://gggenome.dbcls.jp/ja/hg19/>).

### Primer sequences

Name	Primer Sequences
<i>APOE</i> LXRE	Forward 5'- TTT TGT ATT TTT AGT AGA GAT GGG GTT T -3'
	Reverse 5'- AGT AAT ACA GAC ACC CTC CTC CAT T -3'

### Native-PAGE

Cell medium was collected and mixed with 0.1  $\mu$ M PMSF. After centrifugation (800 g, 4°C, 10 min), the supernatant was collected. Sample buffer [200 mM Tris-HCl (pH 6.8), 40%

glycerol, and 0.04% Coomassie brilliant blue R-250] was applied to the sample.

Polyacrylamide gel without SDS was used and kept at 4°C during electrophoresis. The separated proteins were transferred to a 0.4  $\mu$ m PVDF membrane at 4°C for 15 h 20 min. This membrane was blocked with nonfat milk in Tris-buffered saline containing 0.1% Tween-20 and incubated with appropriate primary antibodies at 4°C overnight. Then, HRP-conjugated secondary antibodies were applied to the membrane at room temperature for 1 h. Protein bands were visualized by the enhanced chemiluminescence system using the ChemiDoc™ MP Imaging System. For the densitometric analysis, Image Lab software was used.

### Coimmunoprecipitation using anti-A $\beta$ antibody (4G8)

U87 cells were treated with RXR agonist or SphK2 inhibitor for 48 h. Cell medium was collected and mixed with 0.1  $\mu$ M PMSF. After centrifugation (800 g, 4°C, 10 min), the supernatant was collected as conditioned medium. The solvent for synthetic A $\beta$ <sub>1-42</sub> was replaced from hexafluoro-2-propanol to DMSO immediately before use. Synthetic A $\beta$ <sub>1-42</sub> peptide was applied to the conditioned medium at a final concentration of 1  $\mu$ M and rotated at 4°C overnight. Protein A/G PLUS Agarose (#sc-2003; Santa Cruz Biotechnology) was blocked with 1% BSA/PBS for 1 h and equilibrated with equivalent serum-free medium containing 1% penicillin/streptomycin. Equilibrated beads were mixed with U87 conditioned medium containing 1  $\mu$ M A $\beta$ <sub>1-42</sub>, anti- $\beta$ -Amyloid 17-24 antibody (clone 4G8; BioLegend, San Diego, CA) and Triton X-100, and rotated at 4°C overnight. After centrifugation (1,500 g, 4°C, 3 min), 4G8 wash buffer [50 mM NaCl, 10 mM Tris-HCl (pH 7.6), and 0.01% Triton X-100] was applied to the mixture and rotated at 4°C for 20 min. After additional centrifugation (1,500 g, 4°C, 3 min), 4G8 wash buffer was added to the pellet and resuspended. The mixture was layered on 1 M sucrose/4G8 wash buffer and centrifuged (9,200 g, 4°C, 1 min). Beads were washed with Tris-HCl (pH 7.6) and centrifuged (1,500 g, 4°C, 3 min). Immunoprecipitation samples were boiled in 2 $\times$  SDS sample buffer immediately before use.

*Transferrin uptake.* Reverse-transfected U87 cells were seeded in 12 well plates on poly L-lysine-coated slides. Following day, the medium was replaced with DMEM supplemented with 0.1% BSA without serum and the cells were incubated for 1 h. The cells were then washed twice with PBS and replaced with medium containing Fluorescein (FITC)-conjugated ChromPure Human Transferrin (Jackson Immuno Research Laboratories, Inc., West Grove, PA) diluted to 10  $\mu$ g/ml and incubated at 37°C for 30 min. The cells were preincubated at 4°C for 10 min, and fluorescent transferrin was added in the same manner and incubated at 4°C for 30 min to serve as a control. Cells were washed twice with ice-cold PBS and fixed in PBS containing 4% paraformaldehyde for 30 min. The cells were then incubated with PBS containing 1  $\mu$ g/ml DAPI for 10 min, washed twice with PBS, sealed, and observed using BZ-X800.

### A $\beta$ uptake assay

U87 cells were seeded for the reagent treatment or transfection. One group of cells was treated with reagents for 48 h, and the conditioned medium was collected. The other group of cells was transiently transfected with pFN21AA0816-LRP4-V5-6His vector using PEI MAX (Polysciences, Warrington,

PA) and after 24 h, the medium was changed to serum-free medium containing 1% penicillin/streptomycin and 0.1% BSA. The solvent for synthetic A $\beta$ <sub>1-42</sub> was replaced from hexafluoro-2-propanol to DMSO immediately before use. Synthetic A $\beta$ <sub>1-42</sub> peptide was applied to the conditioned medium at a final concentration of 0.2  $\mu$ M and rotated at 4°C overnight. Then, this medium and lysosome inhibitor, chloroquine (10  $\mu$ M), were applied to LRP4-expressing U87 cells. Cell medium was centrifuged (800 *g*, 4°C, 10 min), and the supernatant was collected. Cells were washed with ice-cold PBS and acid wash solution [0.2 M acetic acid and 0.5 M NaCl] for 6 min and lysed with RIPA buffer. After BCA protein assay, cell medium or lysate samples were boiled in SDS sample buffer and applied to immunoblotting. The densitometric intensity of intracellular ApoE and A $\beta$  was measured as the amount of uptake using Image Lab software.

### Statistical analysis

All experiments were independently repeated at least three times. All data represent mean  $\pm$  SEM. Statistical analysis was performed by two-tailed Student's *t*-test or one-way ANOVA with Dunnett's or Bonferroni's post *hoc* test in GraphPad Prism 8 (GraphPad Software, San Diego, CA; <https://www.graphpad.com/features>). Significance was set at \**P* < 0.05, \*\**P* < 0.01, \*\*\**P* < 0.001, \*\*\*\**P* < 0.0001.

## RESULTS

### SphK2 activation inhibits ApoE induction by LXR/RXR agonists, but not ABCA1

To analyze the physiological function of ApoE and its relationship with SphK2/SIP signaling in astrocytes, we established SphK2 stably overexpressing cells based on human astrocytoma U87 cell line (U87-SphK2 cells), which have the most common genotype of ApoE,  $\epsilon$ 3/ $\epsilon$ 3 (26). We used LXR agonist (T0901317) and RXR agonist (bexarotene) to induce ApoE production. Both agonists induced the expression of ApoE and ABCA1, which mediate the lipidation and secretion of ApoE as a lipoprotein. Interestingly, in U87-SphK2 cells, both agonists induced ABCA1 expression, similar to that in U87-control cells, whereas ApoE induction was strongly suppressed (Fig. 1A–D). We also found that both agonists upregulated the transcription of *APOE* and *ABCA1* in the U87-control cells. However, in U87-SphK2 cells, both agonists induced *ABCA1*, but failed to induce *APOE* transcription (Fig. 1E–I). The SphK2 activity was increased in U87-SphK2 cells (Fig. 1J), indicating that SphK2 activity plays a major role in regulating ApoE expression.

### Endogenous SphK2 activity regulates ApoE expression

To analyze the function of endogenous SphK2, we performed SphK2 knockdown using RNA interference and observed an approximately 60% reduction in SphK2 expression (Fig. 2A, B). In contrast to SphK2 overexpression, SphK2 knockdown resulted in enhanced induction of secreted ApoE by bexarotene (Fig. 2A, C, D), and of secreted and intracellular ApoE

by T0901317 (supplemental Fig. S1A–C). In addition, SphK2 knockdown enhanced *APOE* expression (1.9-fold), but not *ABCA1* at the transcriptional level (Fig. 2E, F). ApoJ (clusterin), like ApoE, is an apolipoprotein abundant in astrocytes. Interestingly, *APOJ* transcription induced by RXR agonist was not affected by SphK2 overexpression or knockdown, suggesting that the effects of SphK2/SIP signaling are ApoE-specific in apolipoproteins (supplemental Fig. S1D, E). To further clarify its correlation with SphK2 activity, we cotreated the cells with bexarotene and SphK2 specific inhibitor, ABC294640 (27). Cotreatment with bexarotene and ABC294640 enhanced the induction of secreted (+1  $\mu$ M ABC: 2.4-fold, +3  $\mu$ M ABC: 4.1-fold) and intracellular (+1  $\mu$ M ABC: 1.5-fold, +3  $\mu$ M ABC: 1.9-fold) ApoE in a dose-dependent manner (Fig. 3A–C). *APOE* mRNA expression was also increased (+ABC: 1.8-fold) but not *ABCA1* by ABC294640 (Fig. 3D, E). In subsequent experiments, we chose the 3  $\mu$ M treatment, which showed a marked increase in ApoE expression, to monitor the effect of ABC294640. In concordance with our finding, another SphK2 specific inhibitor, SLM6031434 (28), also enhanced the induction of ApoE by bexarotene (+0.1  $\mu$ M SLM: 1.1-fold, +0.3  $\mu$ M SLM: 1.2-fold, supplemental Fig. S2A–C). Our data revealed that the transcriptional regulation of ApoE and ABCA1 has distinct aspects and that SphK2 activity plays a key role in ApoE expression.

### Effect of SphK2/SIP signaling on ApoE expression in various astrocyte models

We used human primary astrocytes as another astrocyte model. First, an AAV vector expressing SphK2 under the control of the CMV promoter was transduced, and SphK2 overexpression decreased basal ApoE secretion (0.26-fold) (Fig. 4A–C). We also observed that ApoE secretion was significantly increased by treatment with the SphK2 inhibitor ABC294640 (+ABC: 2.3-fold) (Fig. 4D, E), suggesting that this mechanism is common in astrocytes.

Astrocytes survive and function in the brain through a complex network of other cells, such as neurons and microglia. We examined whether the phenomena observed in U87 cells could be reproduced in a hippocampal slice culture system in which neural circuits are maintained and neurons and glial cells coexist. Furthermore, hippocampal slice cultures have the advantage of easy gene transfer and drug treatment compared with animal models. Hippocampal slices were prepared from 400  $\mu$ m thick sections of postnatal 7–10 days C57BL/6J mice. To specifically express SphK2 in astrocytes, an AAV-GfaABC<sub>1</sub>D-SphK2 vector was generated to express SphK2 under the GfaABC<sub>1</sub>D promoter, which is a truncated GFAP promoter. The GfaABC<sub>1</sub>D promoter has the transcriptional activity similar to that of the GFAP promoter (29). We confirmed that despite the presence of background fluorescence, the staining of expressed SphK2 was

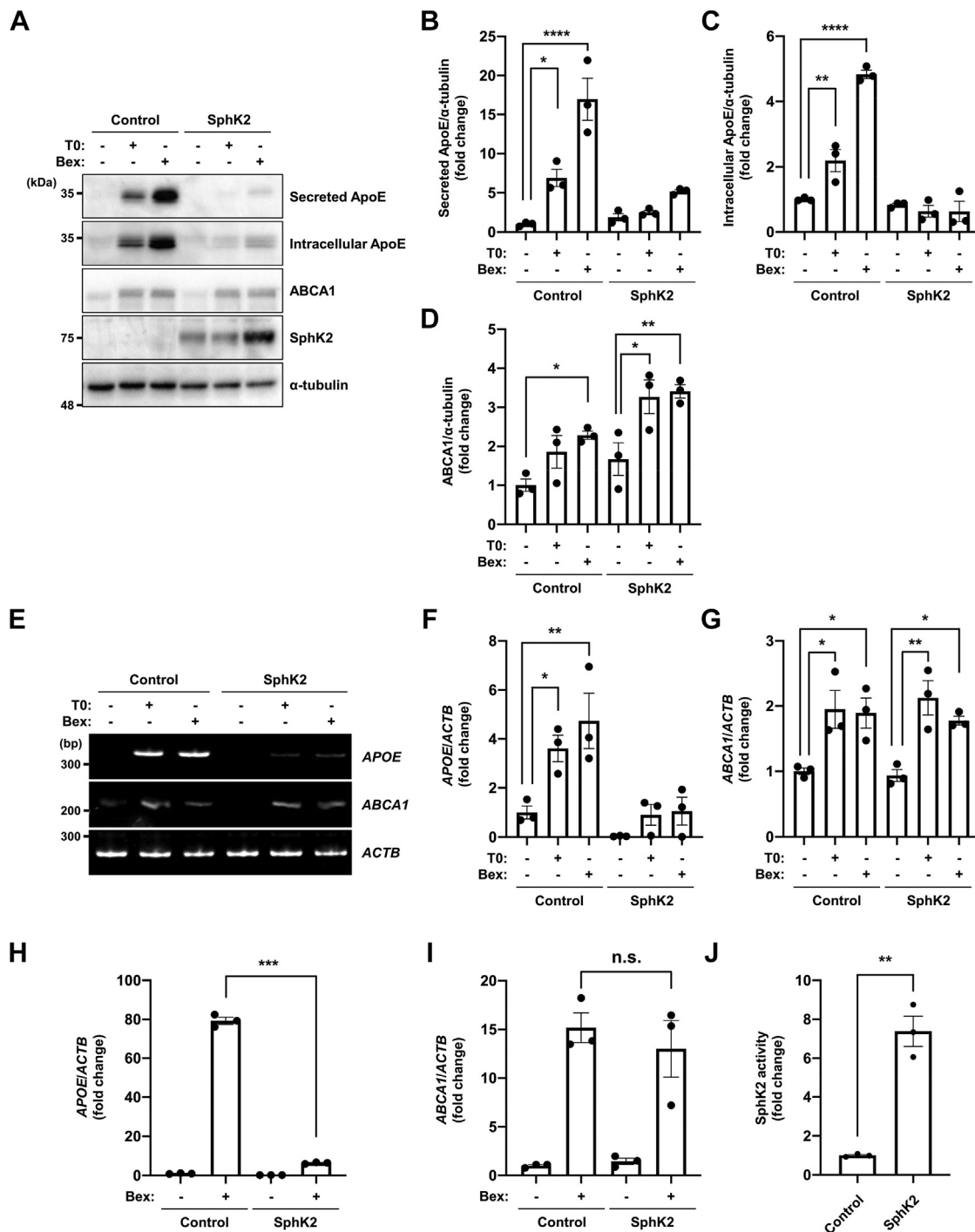


**Fig. 1.** ApoE induction by LXR/RXR agonists is inhibited in U87-SphK2 cells. **A:** Immunoblotting analysis for ApoE, ABCA1, and SphK2 in U87-control and U87-SphK2 cells. Cells were incubated with serum-free medium and treated with 1  $\mu$ M T0901317 (T0) or 1  $\mu$ M bexarotene (Bex) for 48 h. Medium was changed to serum-free 2 h after cell seeding. **B and C:** Quantification of secreted (B) and intracellular (C) ApoE in U87-control and U87-SphK2 cells shown in **Figure 1A**. The relative protein levels were normalized to those of  $\alpha$ -tubulin. Data are expressed as mean  $\pm$  SEM ( $n = 3$ ,  $*P < 0.05$ ,  $**P < 0.01$ ,  $***P < 0.0001$ : significant difference compared with the vehicle sample in U87-control cells by one-way ANOVA with Dunnett's *post hoc* test). **D:** Quantification of ABCA1 in U87-control and U87-SphK2 cells shown in **Figure 1A**. The relative protein levels were normalized to those of  $\alpha$ -tubulin. Data are expressed as mean  $\pm$  SEM ( $n = 3$ ,  $*P < 0.05$ ,  $**P < 0.01$ : significant difference compared with the vehicle sample in U87-control or U87-SphK2 cells by one-way ANOVA with Bonferroni's *post hoc* test). **E:** RT-PCR analysis for *APOE* and *ABCA1* in U87-control and U87-SphK2 cells. Cells were incubated with serum-free medium and treated with 1  $\mu$ M T0901317 or 1  $\mu$ M bexarotene for 48 h. Medium was changed to serum-free 2 h after cell seeding. **F:** Quantification of *APOE* mRNA in U87-control and U87-SphK2 cells shown in **Figure 1E**. The relative mRNA levels were normalized to those of *ACTB*. Data are expressed as mean  $\pm$  SEM ( $n = 3$ ,  $*P < 0.05$ ,  $**P < 0.01$ : significant difference compared with the vehicle sample in U87-control cells by one-way ANOVA with Dunnett's *post hoc* test). **G:** Quantification of *ABCA1* mRNA in U87-control and U87-SphK2 cells shown in **Figure 1E**. The relative mRNA levels were normalized to those of *ACTB*. Data are expressed as mean  $\pm$  SEM ( $n = 3$ ,  $*P < 0.05$ ,  $**P < 0.01$ : significant difference

relatively consistent with GFAP, an astrocyte marker (Fig. 5A). Also, z-stack images indicate that SphK2 is expressed in the nucleus (supplemental Fig. S3). Hippocampal slices were transduced with AAV-GfaABC<sub>1</sub>D-SphK2 at DIV1. In addition, the serum concentration was gradually reduced and replaced with B-27-supplemented Neurobasal-A medium from DIV4 to DIV6 to reduce the reactivity of astrocytes and better simulate in vivo conditions (30). Hippocampal slices were treated with bexarotene and collected at 48 and 96 h post treatment. Although no statistically significant differences were obtained, hippocampal slices over-expressing SphK2 showed a trend toward reduced ApoE induction by bexarotene compared to control slices (Fig. 5B, C). These results suggest that SphK2/SIP signaling regulates ApoE expression in astrocytes and that this mechanism is conserved across species.

### FTY720 inhibits ApoE induction

The next question is whether SIP, a product of SphK2, is a bona fide mediator of the suppression of ApoE expression. Considering that SIP has low cell permeability (31) and is highly unstable (32), we analyzed FTY720, a synthetic analog of sphingosine. FTY720 localizes to the cytoplasm and nucleus after permeabilization of the plasma membrane, and is converted to its SIP analog, FTY720 phosphate (FTY720-P), upon phosphorylation by SphK2 (33). Interestingly, cotreatment with FTY720 and T0901317 markedly reduced the secreted (+1  $\mu$ M FTY: 0.65-fold) and intracellular (+1  $\mu$ M FTY: 0.55-fold) ApoE levels (supplemental Fig. S4A–C).

### SphK2/SIP signaling regulates astrocyte reactivity

Suppression of ApoE expression by SphK2/SIP signaling suggests the possibility of altered astrocyte function. As SphK2/SIP signaling involves in inflammatory responses in multiple cell types, we analyzed the changes in the activity of the NF- $\kappa$ B pathway and the expression of inflammatory cytokines. The subunit p65 of NF- $\kappa$ B was upregulated in U87-SphK2 cells and its translocation to the nucleus was increased (supplemental Fig. S5A). Moreover, interleukin 6 (*IL6*) and *IL1 $\beta$*  mRNA were upregulated in U87-SphK2 cells and SphK2 knockdown decreased their expression (supplemental Fig. S5B–E). These data suggest that

SphK2/SIP signaling exacerbates inflammatory responses in astrocytes. To clarify whether the change in inflammatory status was due to ApoE, we examined basal ApoE levels based on Figure 1H data and found that *APOE* levels were significantly decreased in U87-SphK2 cells (supplemental Fig. S5F). Interestingly, the expression of *IL6* was significantly increased when ApoE was knocked down (supplemental Fig. S5G, H) suggesting that the basal secretion of ApoE has an anti-inflammatory role in astrocytes.

### Nuclear SphK2/SIP signaling regulates RXR $\alpha$ affinity to the target region and its expression

Recently, the nuclear functions of SIP and FTY720-P have attracted attention (34, 35). Interestingly, the nuclear localization of SphK2 is increased in AD brains (36), suggesting a nuclear function of SIP in AD pathogenesis. Nuclear fractionation analysis showed that endogenous and expressed SphK2 is predominantly localized in the nucleus (Fig. 6A, B). Next, we performed a modified ChIP experiment utilizing biotin-avidin conjugation, which allowed for more specific analysis than the antigen–antibody reaction (37). We used the pCAGGS-BLRP-hRXR $\alpha$ -IRES-BirA vector, in which human RXR $\alpha$  was expressed with BLRP at the N terminus, and biotin is recruited to the BLRP by the coexpressed biotin ligase, BirA. U87 cells were transfected with BLRP-hRXR $\alpha$  and after 24 h treated with biotin. The following day, cells were treated with bexarotene for 3 h. The pull-down efficiency of this analysis was confirmed (supplemental Fig. S6). As previously reported (38), bexarotene treatment induced RXR $\alpha$  binding to the target region, around the LXR response element sequence in the *APOE* promoter region in U87-control cells (+bexarotene: 1.35-fold). Interestingly, in U87-SphK2 cells, bexarotene treatment failed to promote RXR $\alpha$  binding to the target region in the *APOE* promoter (Fig. 6C, D). This evidence indicates that nuclear SphK2/SIP functions as a modulator that inhibits RXR $\alpha$  binding to the *APOE* promoter region.

Because SIP and FTY720-P have been reported to function as inhibitors of histone deacetylases (HDAC) (34, 35), we examined the effect of the class I/II HDAC inhibitor, trichostatin A, on ApoE expression. Cotreatment with trichostatin A did not significantly affect ApoE induction by bexarotene (supplemental Fig. S7A,

---

compared with the vehicle sample in U87-control or U87-SphK2 cells by one-way ANOVA with Bonferroni's *post hoc* test). H and I: Quantification of *APOE* (H) and *ABCA1* (I) mRNA in U87-control and U87-SphK2 cells by RT-qPCR analysis. Cells were incubated with serum-free medium and treated with 1  $\mu$ M bexarotene for 48 h. Medium was changed to serum-free 2 h after cell seeding. The relative mRNA levels were normalized to those of *ACTB*. Data are expressed as mean  $\pm$  SEM ( $n = 3$ , \*\*\* $P < 0.001$ : significant difference compared with the bexarotene treatment sample in U87-control cells by one-way ANOVA with Dunnett's *post hoc* test). J: In vitro SphK2 activity in cell lysate. Cells were incubated for 48 h and lysates were collected. The lysates and NBD-sphingosine were mixed, and the alkaline aqueous phase containing NBD-SIP was collected using chloroform/methanol. The NBD-SIP-derived fluorescence was evaluated. Data are expressed as mean  $\pm$  SEM ( $n = 3$ , \*\* $P < 0.01$ : significant difference compared with the control by two-tailed Student's *t*-test). ABCA1, ATP binding cassette transporter A1; ACTB, actin beta; ApoE, apolipoprotein E; NBD, 7-nitro-2,1,3-benzoxadiazole; RT-qPCR, reverse transcription-quantitative PCR; RXR, retinoid X receptor; SIP, sphingosine-1-phosphate; SphK2, sphingosine kinase 2.

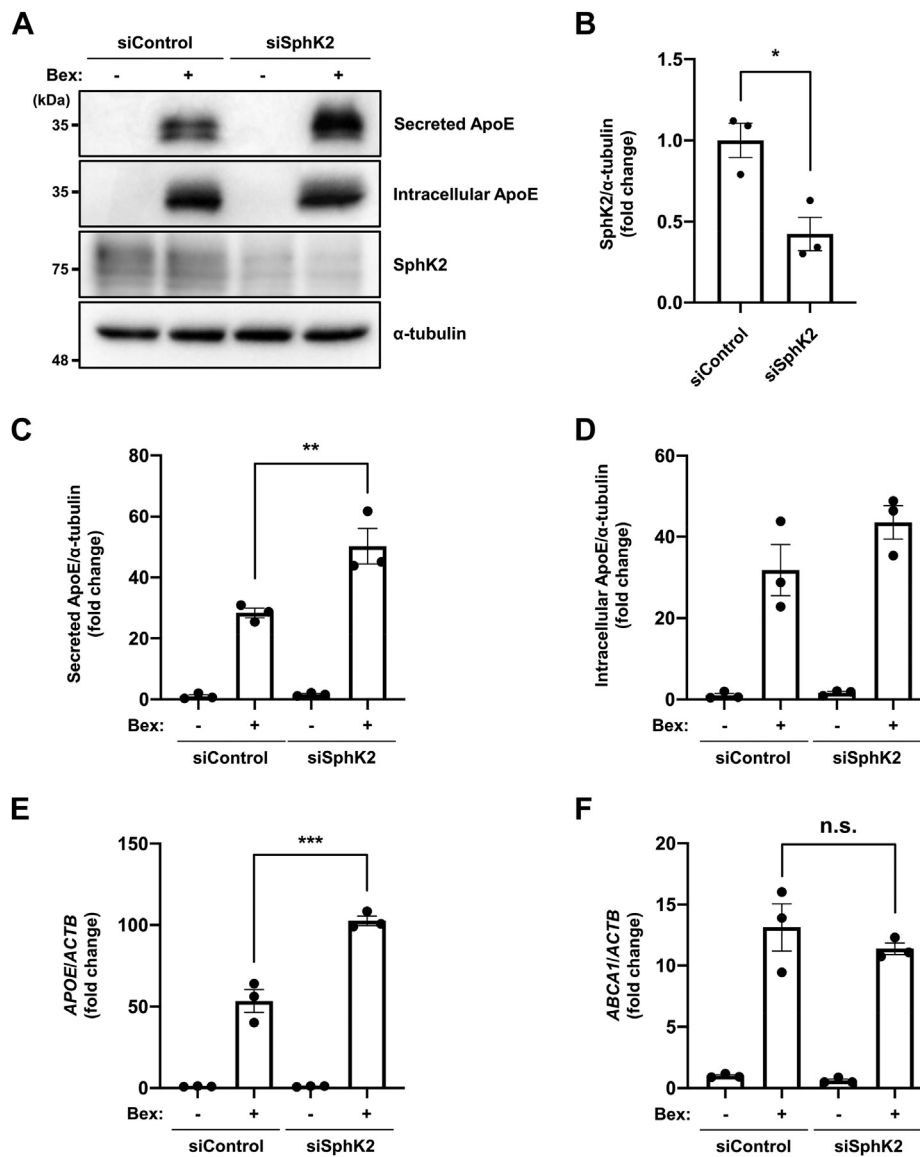


**Fig. 2.** SphK2 knockdown increases ApoE induction by RXR agonist. A: Immunoblotting analysis for ApoE and SphK2 in control and SphK2 siRNA treated cells. U87-control cells were transfected with siRNA and after 24 h, treated with 1  $\mu$ M bexarotene for 48 h. Medium was changed to serum-free 6 h after transfection. B: Quantification of SphK2 knockdown efficiency shown in Figure 2A. The relative protein levels were normalized to those of  $\alpha$ -tubulin. Data are expressed as mean  $\pm$  SEM ( $n = 3$ ,  $*P < 0.05$ : significant difference compared with the control sample by two-tailed Student's *t*-test). C and D: Quantification of secreted (C) and intracellular (D) ApoE in control and SphK2 siRNA treated cells shown in Figure 2A. The relative protein levels were normalized to those of  $\alpha$ -tubulin. Data are expressed as mean  $\pm$  SEM ( $n = 3$ ,  $***P < 0.01$ : significant difference compared with the control sample treated with bexarotene by one-way ANOVA with Dunnett's *post hoc* test). E and F: Quantification of *APOE* (E) and *ABCA1* (F) mRNA in control and SphK2 siRNA treated cells by RT-qPCR analysis. U87-control cells were transfected with siRNA and after 24 h, treated with 1  $\mu$ M bexarotene for 48 h. Medium was changed to serum-free 6 h after transfection. The relative mRNA levels were normalized to those of *ACTB*. Data are expressed as mean  $\pm$  SEM ( $n = 3$ ,  $***P < 0.001$ : significant difference compared with the control sample treated with bexarotene by one-way ANOVA with Dunnett's *post hoc* test). ABCA1, ATP binding cassette transporter A1; ACTB, actin beta; ApoE, apolipoprotein E; RT-qPCR, reverse transcription-quantitative PCR; RXR, retinoid X receptor; SphK2, sphingosine kinase 2.

B), suggesting that HDAC activity is not a major regulator of ApoE expression through SphK2/SIP signaling. Interestingly, as previously reported in all-trans retinoic acid-resistant colon cancer cells, SphK2 overexpression resulted in the downregulation of endogenous RXR $\alpha$  (39), but not of LXR $\alpha$ / $\beta$  (supplemental Fig. S8A–C). Our data suggest that a regulatory mechanism exists between SphK2/SIP signaling and RXR $\alpha$  activity.

### ApoE induced by cotreatment with RXR agonist and SphK2 inhibitor enhances A $\beta$ uptake

Lipidated ApoE has anti-inflammatory effects and promotes A $\beta$  metabolism (12), and SphK2 inhibitor has anti-inflammatory activity in several diseases (40). These lines of evidence indicate that promoting ApoE induction using SphK2 inhibitors may be a therapeutic strategy for AD. To investigate whether ApoE induced by cotreatment with RXR agonist and SphK2 inhibitor

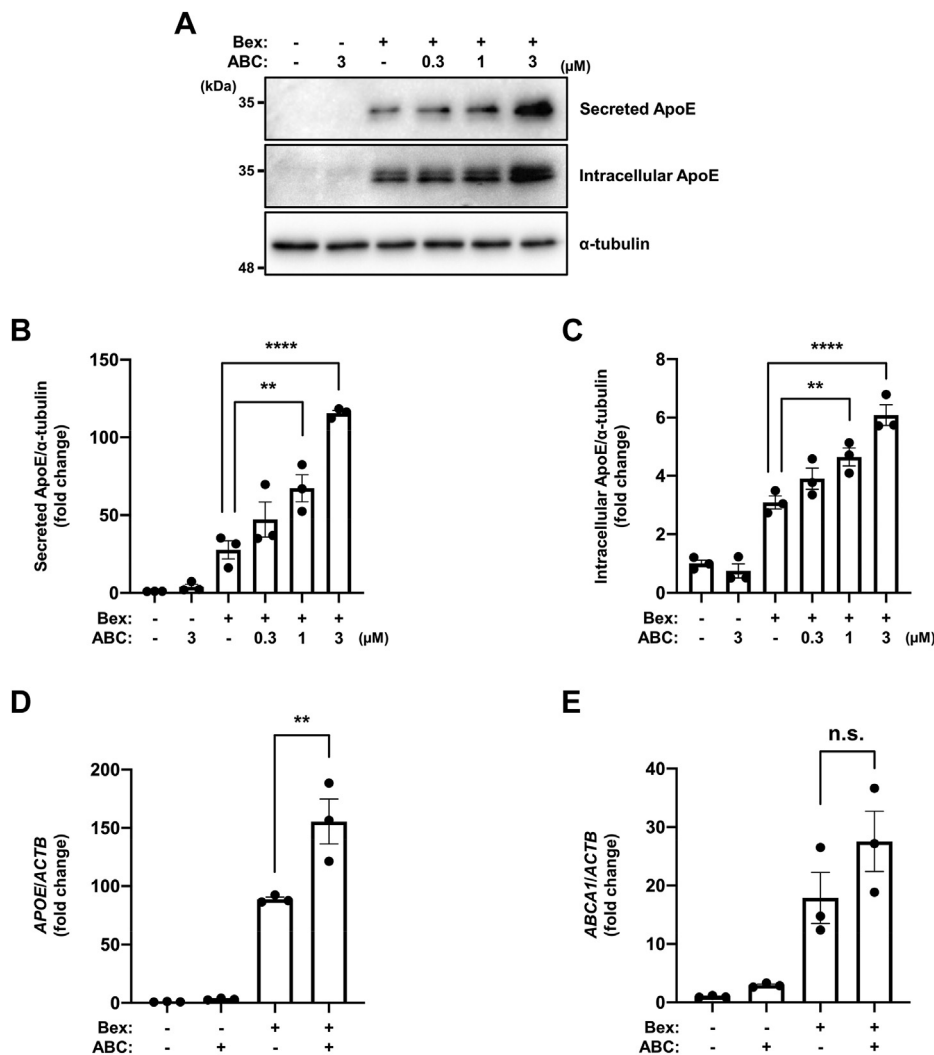


**Fig. 3.** SphK2 inhibitor increases ApoE induction by RXR agonist. **A:** Immunoblotting analysis for ApoE under the SphK2 inhibition condition. U87-control cells were incubated with serum-free medium and treated with 1  $\mu$ M bexarotene and the indicated concentration of ABC294640 (ABC) for 48 h. Medium was changed to serum-free 2 h after cell seeding. **B** and **C:** Quantification of secreted (**B**) and intracellular (**C**) ApoE shown in [Figure 3A](#). The relative protein levels were normalized to those of  $\alpha$ -tubulin. Data are expressed as mean  $\pm$  SEM ( $n = 3$ ,  $**P < 0.01$ ,  $****P < 0.0001$ ; significant difference compared with the bexarotene treatment sample by one-way ANOVA with Dunnett's *post hoc* test). **D** and **E:** Quantification of *APOE* (**D**) and *ABCA1* (**E**) mRNA under the SphK2 inhibition condition by RT-qPCR analysis. U87-control cells were incubated with serum-free medium and treated with 1  $\mu$ M bexarotene and the indicated concentration of ABC294640 for 48 h. Medium was changed to serum-free 2 h after cell seeding. The relative mRNA levels were normalized to those of *ACTB*. Data are expressed as mean  $\pm$  SEM ( $n = 3$ ,  $**P < 0.01$ ; significant difference compared with the bexarotene treatment sample by one-way ANOVA with Dunnett's *post hoc* test). ABCA1, ATP binding cassette transporter A1; ACTB, actin beta; ApoE, apolipoprotein E; RT-qPCR, reverse transcription-quantitative PCR; RXR, retinoid X receptor; SphK2, sphingosine kinase 2.

is properly lipidated, we performed native-PAGE analysis. We found that the induced ApoE was similarly lipidated (41, 42), with or without the SphK2 inhibitor ([Fig. 7A](#)). Next, to examine the interaction between lipidated ApoE and A $\beta$ , we incubated conditioned medium from reagent-treated U87 cells with synthetic A $\beta_{1-42}$  overnight. Coimmunoprecipitation analysis using A $\beta$  antibody (4G8) revealed that lipidated ApoE could interact with A $\beta$  ([Fig. 7B, C](#)). Although the interaction level was similar with or without SphK2 inhibitor, we hypothesized that lipidation status might alter the ApoE and A $\beta$  uptake into the astrocytes. To check this possibility, we focused on LRP4, the major

ApoE receptor in astrocytes, to promote A $\beta$  clearance (43). We verified that endocytosis during LRP4 expression was not apparently different from that in the controls using FITC-transferrin ([supplemental Fig. S9](#)). The LRP4-V5-6His vector was transiently expressed in U87 cells, and the medium was replaced with one that promotes the ApoE-A $\beta$  complex formation as shown in [Figure 7B](#). Chloroquine was also added to reduce lysosomal degradation. We found that medium from SphK2 inhibitor cotreatment significantly promoted ApoE (1.71-fold) and A $\beta$  (2.13-fold) uptake into cells compared with bexarotene treatment alone ([Fig. 7D-F](#)). These results suggest that RXR agonists and

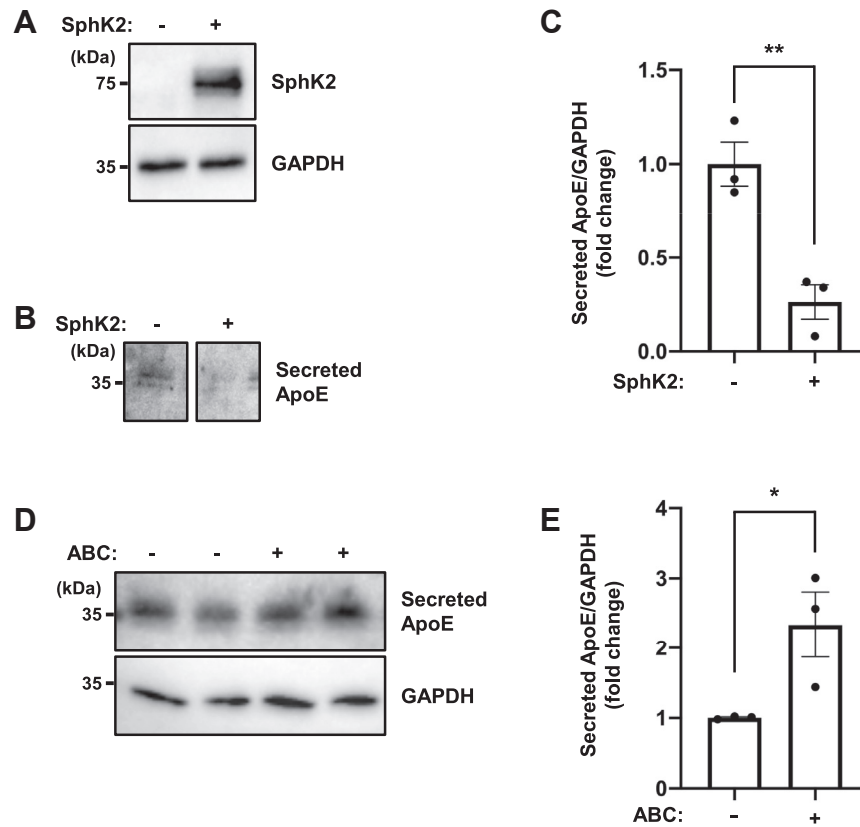


**Fig. 4.** SphK2/SIP signaling regulates ApoE expression in human primary astrocytes. A and B: Immunoblotting analysis for SphK2 (A) and secreted ApoE (B). Human primary astrocytes were transduced with AAV2-CMV-SphK2. Following day, the medium was changed to serum-free and incubated for 48 h. C: Quantification of secreted ApoE shown in Figure 4B. The relative protein levels were normalized to those of GAPDH. Data are expressed as mean  $\pm$  SEM ( $n = 3$ ,  $**P < 0.01$ : significant difference compared with the control sample by two-tailed Student's  $t$ -test). D: Immunoblotting analysis for secreted ApoE. Human primary astrocytes were treated with 3  $\mu$ M ABC294640 for 48 h in serum-free condition. E: Quantification of secreted ApoE shown in Figure 4D. The relative protein levels were normalized to those of GAPDH. Data are expressed as mean  $\pm$  SEM ( $n = 3$ ,  $*P < 0.05$ : significant difference compared with the vehicle sample by two-tailed Student's  $t$ -test). AAV, adeno-associated virus; ApoE, apolipoprotein E; ApoE, apolipoprotein E; CMV, cytomegalovirus; SIP, sphingosine-1-phosphate; SphK2, sphingosine kinase 2.

SphK2 inhibitors can improve A $\beta$  metabolism in a concerted manner.

## DISCUSSION

Alterations in lipid composition significantly affect the AD pathology, particularly through changes in astrocyte function. Interestingly, the expression of ApoE, which regulates lipid homeostasis, is down-regulated in astrocytes in AD (9, 10), which is suggestive of a vicious cycle between abnormal lipid metabolism and aberrant astrocyte function. Furthermore, because ApoE has anti-inflammatory and A $\beta$ -metabolizing effects, increasing ApoE levels may have therapeutic effects on AD. Based on this notion, the induction of ApoE expression by the activation of the nuclear receptors, RXR and LXR, has attracted the attention of researchers. In particular, the therapeutic effect of bexarotene, an RXR agonist, on AD has been well studied, but its effects differ among research groups, suggesting the presence of factors related to AD

pathophysiology that modulate the expression or function of ApoE.

Here, we focused on the SphK2/SIP pathway, a lipid signaling pathway, which we previously showed to be activated in AD pathology (17). The signaling lipid SIP is involved in high-density lipoprotein (HDL) function (44) and neuroinflammation through the regulation of gene expression in the nucleus and alteration in the functioning of various immune cells (45). Because ApoE, a risk factor for AD, functionally overlaps with SIP in its involvement in lipid metabolism, neuro-inflammatory functions, and related diseases (46), we analyzed the relationship between the two molecules using several astrocyte models. In this study, we analyzed the most common isoform, ApoE3, with the aim of elucidating its functional regulation. Interestingly, we showed that upregulation of SphK2 activity suppressed the induction of ApoE, but not of ABCA1 and ApoJ, by both RXR and LXR agonists at the transcriptional level. We also found that the binding of RXR $\alpha$  to the *APOE* promoter region is suppressed upon

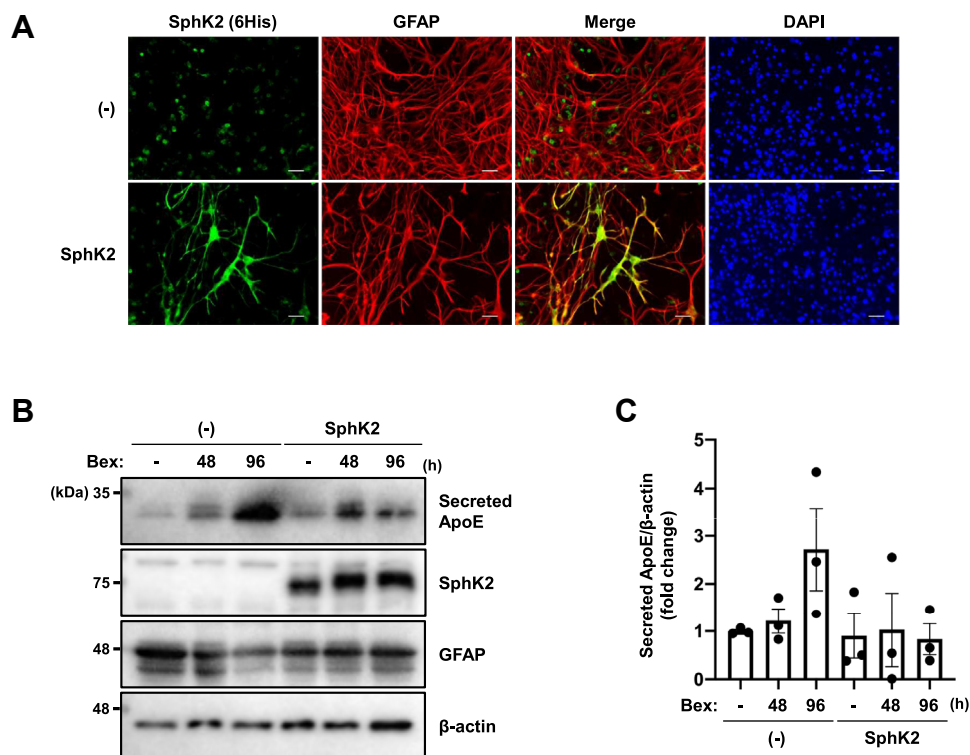


**Fig. 5.** SphK2/SIP signaling tends to suppress ApoE expression in hippocampal slices. **A:** Immunostaining of hippocampal slice. V5-6His tagged SphK2 (green) and astrocytic marker GFAP (red) were detected. DAPI stained the nucleus (blue). Slices were incubated with serum-free medium consisting of MEM, HBSS, and B-27-supplemented Neurobasal-A and analyzed at DIV11. Scale bars represent 30  $\mu\text{m}$ . **B:** Immunoblotting analysis for ApoE, SphK2, and GFAP in hippocampal slices. Slices were transduced with AAV2-GfaABC<sub>1</sub>D-SphK2 at DIV1. The slices were incubated with serum-free medium consisting of MEM, HBSS, and B-27-supplemented Neurobasal-A. At DIV7, the slices were treated with DMSO for 96 h or 1  $\mu\text{M}$  bexarotene for 48 and 96 h. The medium was gradually changed to serum-free from DIV4 to 6. **C:** Quantification of secreted ApoE shown in Figure 5B. The relative protein levels were normalized to those of  $\beta$ -actin. Data are expressed as mean  $\pm$  SEM ( $n = 3$ , significant difference compared with the vehicle sample by one-way ANOVA with Dunnett's *post hoc* test). AAV, adeno-associated virus; ApoE, apolipoprotein E; DAPI, 4',6-diamidino-2-phenylindole; DIV, days in vitro; GFAP, glial fibrillary acidic protein; HBSS, Hanks' balanced salt solution; MEM, minimum essential medium; SIP, sphingosine-1-phosphate; SphK2, sphingosine kinase 2.

SphK2 activation, suggesting the pivotal role of nuclear SIP. Intriguingly, the suppression of SphK2 activity by knockdown or inhibitors upregulated the induction of ApoE and facilitated A $\beta$  uptake in astrocytes. Considering our previous findings that SphK2 activity is upregulated in AD brain and promotes A $\beta$  production in neurons, suppression of SphK2/SIP signaling may be a promising multifunctional therapeutic strategy for AD that can act on both astrocytes and neurons.

Of the two SphK isozymes, SphK2 is predominant in the brain (47). We found a strong correlation between SphK2/SIP activity and ApoE expression; increased SphK2 activity suppressed ApoE expression, and conversely, SphK2 knockdown or inhibitors promoted ApoE expression by RXR or LXR agonist but did not affect ABCA1 and ApoJ expression (Figs. 1–3 and supplemental Fig. S1). ApoJ is one of the main apolipoproteins in the brain and its expression is reported to be upregulated in AD (48). Although the function of ApoJ in AD is not fully understood, the fact that apolipoprotein balance is altered by SphK2/SIP signaling is intriguing and is a subject for future investigation. ApoE regulation by SphK2/SIP signaling was observed in

human primary astrocytes and cultured hippocampal slices, suggesting that this mechanism is reproducible in several astrocyte models (Figs. 4 and 5). SIP, a product of SphK2, mainly functions as an extracellular ligand for G protein-coupled receptors and as a transcriptional regulator in the nucleus (49). The sphingosine analog, FTY720, is phosphorylated by SphK2 to produce the SIP analog, FTY720-P. In contrast to SIP, FTY720-P modulates SIP receptors (SIPRs) to reduce their cell surface expression and signaling (50). We found that FTY720 suppressed ApoE induction (supplemental Fig. S4). Considering the effect of SphK2/SIP signaling on *APOE* transcription (Figs. 1–3 and supplemental Fig. S1), the nuclear function of SIP itself is strongly involved in ApoE regulation. Interestingly, we have previously shown that FTY720 increases A $\beta$ <sub>42</sub> levels in AD model mice (51), and regulation of ApoE expression in astrocytes might be involved and needs to be explored further. However, this study cannot fully deny the non-nuclear function of SphK2/SIP signaling. Indeed, the levels of SIP<sub>3</sub> receptor are increased and this receptor has been reported to be involved in the induction of inflammation in reactive astrocytes (52). The possibility

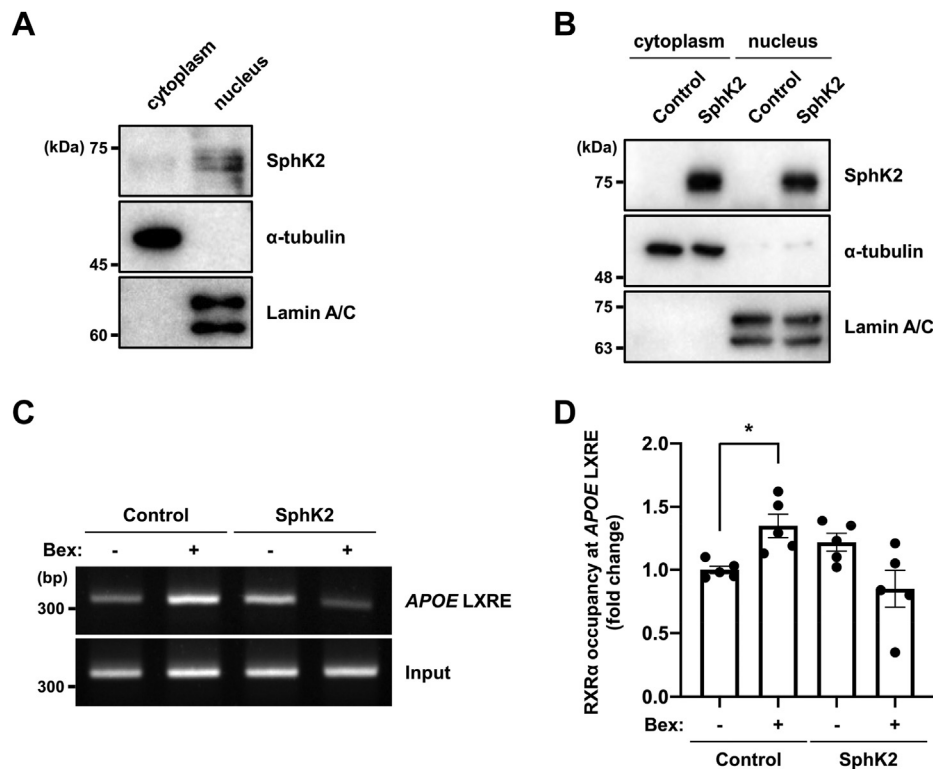


**Fig. 6.** Nuclear SphK2/SIP signaling alters RXR $\alpha$  affinity to the *APOE* promoter. A and B: Nuclear fractionation analysis for SphK2. Endogenous (A) and expressed (B) SphK2 were detected in U87 cells.  $\alpha$ -tubulin and Lamin A/C were used as cytoplasm and nuclear marker protein, respectively. C: ChIP analysis for RXR $\alpha$  binding to the *APOE* promoter region. U87-control and U87-SphK2 cells were transfected with pCAGGS-BLRP-hRXR $\alpha$ -IRES-BirA and after 24 h, treated with 50  $\mu$ g/ml D-biotin along with medium change to serum-free condition. Following day, cells were treated with 1  $\mu$ M bexarotene for 3 h. D: Quantification of RXR $\alpha$  occupancy at the *APOE* promoter region shown in Figure 6C. The relative levels of the enrichment of RXR $\alpha$  on the *APOE* promoter were normalized to those of input. Data are expressed as mean  $\pm$  SEM ( $n = 5$ ,  $*P < 0.05$ ; significant difference compared with the vehicle sample in U87-control cells by one-way ANOVA with Dunnett's *post hoc* test). ApoE, apolipoprotein E; BLRP, biotin ligase recognition peptide; ChIP, chromatin immunoprecipitation; LXRE, LXR response element; RXR, retinoid X receptor; SIP, sphingosine-1-phosphate; SphK2, sphingosine kinase 2.

remains that SIPR signaling, in addition to the nuclear function of SphK2/SIP signaling, cooperatively contributes to altered astrocyte function in AD. Another concern is that in SphK2-expressing hippocampal slices and U87-SphK2 cells, SphK2 was highly localized in the cytoplasm (supplemental Fig. S3 and Fig. 6B). Since SIP is known to shuttle between the cytoplasm and the nucleus, this study leaves open the possibility that SIP acts in the cytoplasm. The nuclear function of SphK2 has been verified in other studies, and further analysis of the function of nuclear SIP will be needed to test our hypothesis in more detail, using the nuclear localization-related mutants described in those articles (53, 54). In addition, our study suggests a correlation between increased SIP and suppressed ApoE expression, but the overall sphingolipid changes were not analyzed. Therefore, this aspect should be investigated in the future.

Interestingly, SphK2/SIP signaling regulated the inflammatory response in astrocytes (supplemental Fig. S5). In particular, activation of the NF- $\kappa$ B pathway by increased SphK2 expression was similar to that observed in regorafenib-resistant hepatocellular carcinoma-derived cells (55). SphK2 expression and

nuclear translocation of p65 were increased in these cells. Moreover, *IL6* and *IL1 $\beta$*  expression increased in U87-SphK2 cells (supplemental Fig. S5B, C). Interestingly, activation of the NF- $\kappa$ B pathway by ApoE knockout has also been reported (56). We found that basal *ApoE* levels decreased in U87-SphK2 cells, and ApoE knockdown increased *IL6* expression (supplemental Fig. S5F–H). Considering that SIP and ApoE have proinflammatory and anti-inflammatory effects, respectively, SphK2/SIP signaling may regulate the inflammatory response through the regulation of basal ApoE in astrocytes. However, this study was not able to show a direct relationship between the two, so future verification is needed. In addition, the antitumor effects of SphK2 inhibitors and ApoE have also been reported, so it will be interesting to analyze the relationship between the two in this aspect.

The mechanism underlying the regulation of ApoE expression by SphK2/SIP signaling was not fully elucidated in this study, although there are some clues. Accumulating evidence indicates the importance of SIP as a transcriptional regulator. We confirmed that endogenous SphK2 is predominantly distributed in the

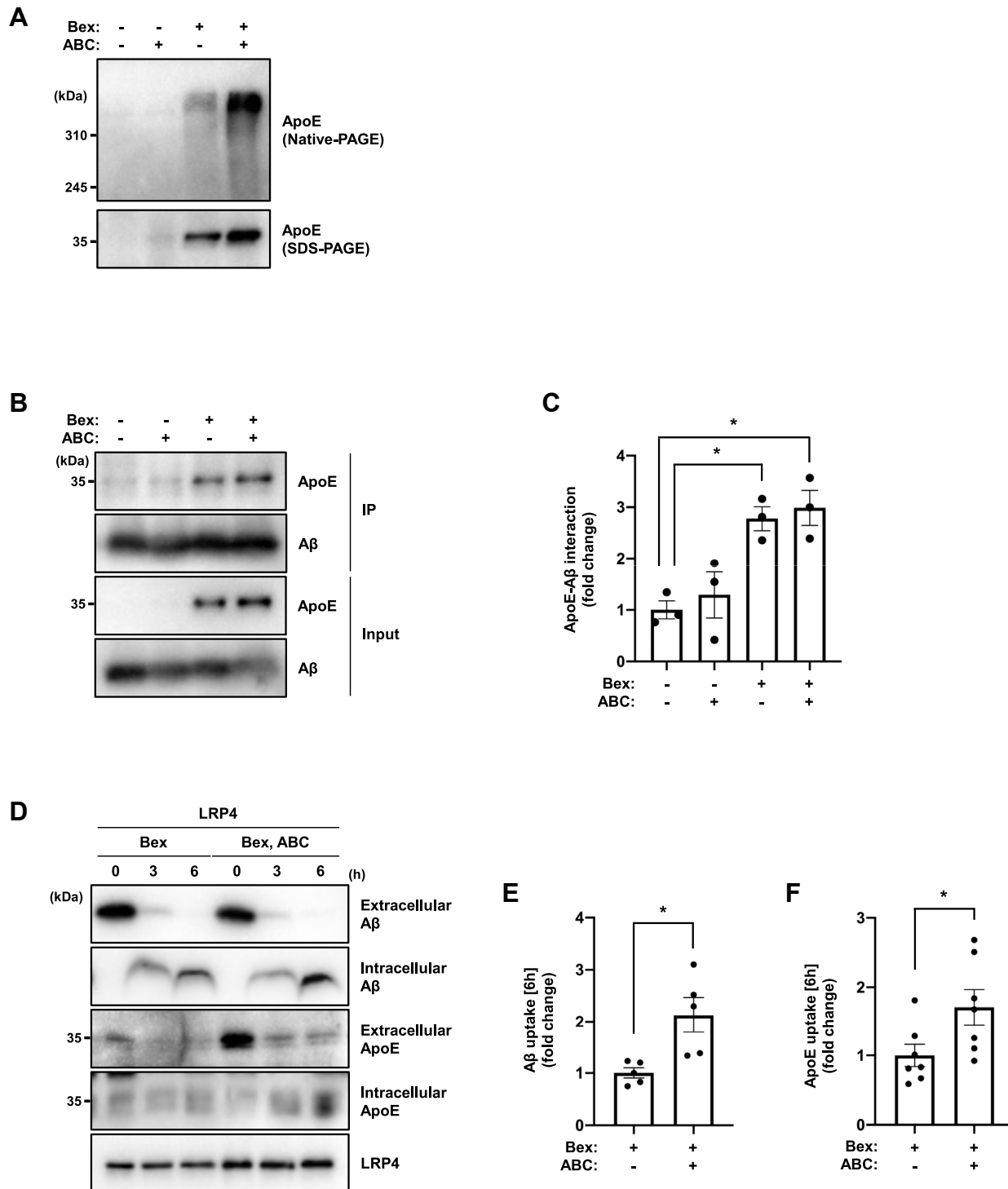


**Fig. 7.** SphK2 inhibitor enhances A $\beta$  uptake in astrocytes. **A:** Native-PAGE (top) and SDS-PAGE (bottom) analysis for ApoE. U87-control cells were incubated with serum-free medium and treated with 1  $\mu$ M bexarotene and 3  $\mu$ M ABC294640 for 48 h. Medium was changed to serum-free 2 h after cell seeding. **B:** Coimmunoprecipitation analysis using A $\beta$  antibody (4G8). U87-control cells were incubated with serum-free medium and treated with 1  $\mu$ M bexarotene and 3  $\mu$ M ABC294640 for 48 h. Then the conditioned medium was incubated with 1  $\mu$ M synthetic A $\beta$ <sub>1-42</sub> at 4°C overnight. **C:** Quantification of secreted ApoE-A $\beta$  interaction shown in Figure 7B. Data are expressed as mean  $\pm$  SEM ( $n = 3$ ,  $*P < 0.05$ : significant difference compared with the vehicle sample by one-way ANOVA with Dunnett's *post hoc* test). **D:** A $\beta$  uptake assay in LRP4-expressing U87 cells. U87-control cells were transfected with pFN21AA0816-LRP4-V5-6His and incubated with the medium in which ApoE-A $\beta$  interaction is detected shown in Figure 7B for 6 h. **E and F:** Quantification of intracellular A $\beta$  (E) and ApoE (F) shown in Figure 7D. Data are expressed as mean  $\pm$  SEM ( $n = 5-7$ ,  $*P < 0.05$ : significant difference compared with the bexarotene treatment sample by two-tailed Student's *t*-test). A $\beta$ , amyloid  $\beta$ ; ApoE, apolipoprotein E; LRP4, lipoprotein receptor-related protein 4; SphK2, sphingosine kinase 2.

nucleus, and its expression level is increased in U87-SphK2 cells (Fig. 6A, B). Although SIP has been reported to repress HDAC activity (34), treatment with an HDAC inhibitor did not affect ApoE production by RXR agonist (supplemental Fig. S7). In addition, because HDAC inhibition has been reported to increase ApoE expression (57), it is unlikely that histone acetylation is involved in this mechanism.

Another hypothesis involves functional regulation of RXR/LXR. The results of ChIP experiments targeting the binding site of RXR $\alpha$  indicated that SphK2/SIP signaling regulates the nuclear RXR $\alpha$  activity (Fig. 6C, D). We also analyzed the expression of nuclear receptors and showed that RXR $\alpha$  expression is decreased in U87-SphK2 cells (supplemental Fig. S8), consistent with previous studies in colon cancer resistant to all-trans retinoic acid, the RXR agonist (39). In contrast, there was no effect of SphK2 overexpression on LXR $\alpha/\beta$  expression (supplemental Fig. S8). Interestingly, RXR $\alpha$  expression is downregulated in AD model mice (58). Considering that the RXR/LXR heterodimer is activated by RXR agonists alone, SphK2/SIP signaling might act on RXR $\alpha$  directly or indirectly. Since ABCA1, which is also regulated by RXR, is not affected (Figs. 1–3), it is unlikely that the reduced RXR $\alpha$  expression is sufficient to define the expression level of ApoE, and a more complex mechanism is expected.

There are several possible mechanisms underlying the specificity of ApoE. First, the difference in the transcriptional mechanism between *APOE* and *ABCA1* is that *APOE* expression is induced by complex formation with RXR and several transcription factors, not only on the promoter but also on the enhancer region (59, 60), and regulation of the expression of *ABCA1* is simpler than that of *APOE* (61). SphK2/SIP may inhibit the formation of ApoE-specific transcription factor complexes. The second mechanism is a conformational change in RXR $\alpha$ . Recently, modulators that alter the conformation of nuclear receptors, thereby modulating their function, have attracted considerable attention (62). Interestingly, the effects of SIP on nuclear receptors, such as peroxisome proliferator-activated receptor  $\gamma$  (63), are gradually being revealed, and it will be necessary to verify whether SIP directly affects the conformation and activity of RXR $\alpha$ .

A role for SphK2/SIP signaling in AD has been proposed. We have shown an increase in SphK2 activity in the frontal cortex of AD brains (17). Notably, Lei *et al.* reported that SphK2 KO J20 mice have decreased A $\beta$  aggregation (19). Another group, using mice deficient in SGPL1, an irreversible SIP-degrading enzyme, reported that SIP accumulation induces neurodegeneration, tau pathology, and astrogliosis (18, 64). However, some groups have shown a reduction in SphK2 activity or SIP levels in AD (65, 66). It is important to discuss these conflicting findings, including the localization of SphK2. SphK2 has both nuclear localization and export signals for shuttling between the cytoplasm and nucleus

in response to the cellular environment (53). Cytoplasmic SphK2-derived SIP has cytoprotective effects, such as promoting cell survival; however, under stress conditions, such as high cell density or serum starvation, it accumulates in the nucleus (53, 67). Indeed, the nuclear accumulation of SphK2 has been reported in AD brains (36), suggesting that the harmful effect of nuclear SIP plays an important role in AD pathogenesis. Our results may facilitate the development of novel AD treatment strategies. However, SphK2 KO J20 mice showed hippocampal volume loss, myelin loss, and cognitive impairment (19); therefore, the possibility of adverse effects should be considered.

Lipidated ApoE exists extracellularly as HDL-like particles. SIP is incorporated into HDL-like particles in an ABCA1-dependent manner and coexists with ApoE (44). These particles regulate various physiological functions, such as A $\beta$  uptake via ApoE receptors and cell migration via SIPRs (68, 69). ApoE secreted upon cotreatment with RXR agonist and SphK2 inhibitor was lipidated as in the case of treatment with RXR agonist alone (Fig. 7A). Although the efficiency of binding between ApoE and A $\beta$  was not significantly different (Fig. 7B, C), we hypothesized that ApoE induced by cotreatment with RXR agonist and SphK2 inhibitor would form lipid particles lacking SIP and would alter its function.

In this study, we focused on the ApoE receptor, LRP4. LRP4 is the most abundant among the LDLR family members known as ApoE receptors in astrocytes (70). Furthermore, LRP4 is downregulated in the hippocampus, cortex, and entorhinal cortex of AD patients, and amyloid pathology is exacerbated in 5xFAD mice lacking LRP4, suggesting an important role for LRP4 in A $\beta$  metabolism (43). In the present study, we found that cotreatment with RXR agonist and SphK2 inhibitor significantly enhanced uptake of A $\beta$  as well as ApoE in LRP4-expressing astrocytes, suggesting a protective effect via enhancement of A $\beta$  metabolism (Fig. 7D–F). We also demonstrate that the combination of an RXR agonist and a SphK2 inhibitor is effective for the treatment of AD. In this study, chloroquine was used to evaluate uptake, which does not fully reflect physiological conditions because A $\beta$  is inherently degraded. While this analysis has revealed an enhancement effect of A $\beta$  uptake, it will be necessary to clarify the relationship between LRP4 and A $\beta$  under pathological conditions, such as in AD model mice in the future. Bexarotene has shown therapeutic effects in AD model mice (11), and clinical trials have shown reduction in cortical amyloid levels, although side effects, particularly triglyceride accumulation, have been observed (71). However, the effects of bexarotene have been variable in most follow-up studies (13–16), suggesting that certain factors cause these variations. Our results suggest that enhanced SphK2/SIP signaling may be a contributing factor. Moreover, SphK2 inhibitors may compensate for the effects of bexarotene, requiring lower doses and fewer adverse effects.

ApoE has three isoforms—ApoE2, ApoE3, and ApoE4—with ApoE3 being the most common. Although the products of these gene variants differ by only one or two amino acid residues, these small differences have profound effects on binding to A $\beta$ , ApoE receptors, and lipids (46). In particular, ApoE4 is known to be the strongest genetic risk factor for sporadic AD, and the number of  $\epsilon$ 4 genes affects the risk and accelerates the onset of AD (72). Interestingly, bexarotene has been shown to be less effective against ApoE4 carriers than noncarriers (71). In addition, it has been reported that the promotion of ApoE4 lipidation suppresses ApoE4-driven pathology (42, 73). Similarly, SphK2 inhibitors increase lipidated ApoE levels and may also promote A $\beta$  metabolism under ApoE4 conditions. However, it has been reported that ApoE4 promotes AD pathology through toxic gain of function (74). As our study focused on ApoE3, we must investigate the effect of ApoE4 in the treatment of AD.

In conclusion, in this study, we demonstrate the importance of nuclear SIP in astrocyte function. It may work in concert with known therapeutic targets, RXR and LXR agonists, to increase ApoE and improve astrocyte function, potentially expanding treatment options. Furthermore, considering our previous studies (17), SphK2/SIP signaling is a potential target for multitargeted therapy, that is, A $\beta$  production in neurons and A $\beta$  metabolism via the regulation of ApoE expression in astrocytes. Although the relationship between nuclear lipid function and AD pathogenesis remains unclear, this study may provide a clue to this question, and a comprehensive search for nuclear SIP-binding proteins in the future will be useful in understanding the functional changes of astrocytes in AD.

### Data Availability

All data are contained within the article and the [supporting information](#). All data reported in this manuscript will be shared by the lead contact upon request. Raw data of immunoblotting, RT-PCR and ChIP in main figures are deposited on <https://doi.org/10.17632/rb89bxdhwj.2>. 

### Supplemental data

This article contains [supplemental data](#).

### Acknowledgments

We are grateful to Dr T. Tomita, Dr T. Hashimoto, and Dr R. Koyama (Tokyo University) for providing plasmids and technical advice. We thank H. Nakai, M. Matsumoto, and K. Sueyoshi for technical assistance and H. Kurogi for help in creating graphical abstract. We also thank Editage ([www.editage.jp](http://www.editage.jp)) for English language editing.

### Author contributions

M. K., Y. N., A. I., N. K., Y. K., and N. T. investigation; M. K., Y. N., A. I., N. K., Y. K., and N. T. formal analysis; M. K., Y. N., N. K., and N. T. methodology; M. K., T. S., and N. T. funding

acquisition; M. K. and N. T., conceptualization; M. K. and N. T. writing—original draft; A. I., N. K., Y. K., T. S., T. U. and N. T. writing—review and editing; Y. K., T. S., T. U., and N. T. supervision; T. S. and T. U. resources; N. T. project administration.

### Author ORCIDs

Nanaka Kaneshiro  <https://orcid.org/0000-0003-4452-2655>

Yuji Kamikubo  <https://orcid.org/0000-0003-1985-5212>

Takashi Sakurai  <https://orcid.org/0000-0001-9515-6574>

Takashi Uehara  <https://orcid.org/0000-0002-6562-2957>

Nobumasa Takasugi  <https://orcid.org/0000-0002-6059-2082>

### Funding and additional information

This work was supported by the Grant-in-Aid for Scientific Research (C) from the Japan Society for the Promotion of Science (26430059, 17K08272, and 20K07014 to N. T.), Scientific Research (B) (21H02815 to T. S.), JST, the establishment of university fellowships toward the creation of science technology innovation (JPMJFS2128), and Grant-in-Aid for JSPS Fellows (23KJ1603) (to M. K.).

### Conflict of interest

The authors declare that they have no conflicts of interest with the contents of this article.

### Abbreviations

AAV, adeno-associated virus; A $\beta$ , amyloid  $\beta$ ; ABCA1, ATP binding cassette transporter A1; ACTB, actin beta; AD, Alzheimer's disease; BLRP, biotin ligase recognition peptide; ChIP, chromatin immunoprecipitation; CMV, cytomegalovirus; DIV, days in vitro; GFAP, glial fibrillary acidic protein; HDAC, histone deacetylase; HDL, high-density lipoprotein; HEK, human embryonic kidney; IL, interleukin; LRP4, low-density lipoprotein receptor-related protein 4; NBD, 7-nitro-2,1,3-benzoxadiazole; NF- $\kappa$ B, nuclear factor- $\kappa$ B; qPCR, quantitative PCR; RXR, retinoid X receptor; SIP, sphingosine-1-phosphate; SIPR, sphingosine-1-phosphate receptor; SphK2, sphingosine kinase 2.

Manuscript received October 24, 2023, and in revised form January 11, 2024. Published, JLR Papers in Press, January 26, 2024, <https://doi.org/10.1016/j.jlr.2024.100510>

## REFERENCES

1. Hardy, J., and Selkoe, D. J. (2002) The amyloid hypothesis of Alzheimer's disease: progress and problems on the road to therapeutics. *Science* **297**, 353–356
2. Scheltens, P., De Strooper, B., Kivipelto, M., Holstege, H., Chételet, G., Teunissen, C. E., et al. (2021) Alzheimer's disease. *Lancet* **397**, 1577–1590
3. van Dyck, C. H., Swanson, C. J., Aisen, P., Bateman, R. J., Chen, C., Gee, M., et al. (2023) Lecanemab in early Alzheimer's disease. *N. Engl. J. Med.* **388**, 9–21
4. Guzman-Martinez, L., Maccioni, R. B., Andrade, V., Navarrete, L. P., Pastor, M. G., and Ramos-Escobar, N. (2019) Neuroinflammation as a common feature of neurodegenerative disorders. *Front. Pharmacol.* **10**, 1008
5. Liddel, S. A., Guttenplan, K. A., Clarke, L. E., Bennett, F. C., Bohlen, C. J., Schirmer, L., et al. (2017) Neurotoxic reactive astrocytes are induced by activated microglia. *Nature* **541**, 481–487

6. Barber, C. N., and Raben, D. M. (2019) Lipid metabolism crosstalk in the brain: Glia and neurons. *Front. Cell. Neurosci.* **13**, 212
7. Bellaver, B., Povala, G., Ferreira, P. C. L., Ferrari-Souza, J. P., Leffa, D. T., Lussier, F. Z., et al. (2023) Astrocyte reactivity influences amyloid- $\beta$  effects on tau pathology in preclinical Alzheimer's disease. *Nat. Med.* **29**, 1775–1781
8. Guttenplan, K. A., Weigel, M. K., Prakash, P., Wijewardhane, P. R., Hasel, P., Rufen-Blanchette, U., et al. (2021) Neurotoxic reactive astrocytes induce cell death via saturated lipids. *Nature* **599**, 102–107
9. Mathys, H., Davila-Velderrain, J., Peng, Z., Gao, F., Mohammadi, S., Young, J. Z., et al. (2019) Single-cell transcriptomic analysis of Alzheimer's disease. *Nature* **570**, 332–337
10. Grubman, A., Chew, G., Ouyang, J. F., Sun, G., Choo, X., McLean, C., et al. (2019) A single-cell atlas of entorhinal cortex from individuals with Alzheimer's disease reveals cell-type-specific gene expression regulation. *Nat. Neurosci.* **22**, 2087–2097
11. Cramer, P. E., Cirrito, J. R., Wesson, D. W., Lee, C. Y. D., Karlo, J. C., Zinn, A. E., et al. (2012) ApoE-directed therapeutics rapidly clear  $\beta$ -amyloid and reverse deficits in AD mouse models. *Science* **335**, 1503–1506
12. Jiang, Q., Lee, C. Y. D., Mandrekar, S., Wilkinson, B., Cramer, P., Zelcer, N., et al. (2008) ApoE promotes the proteolytic degradation of A $\beta$ . *Neuron* **58**, 681–693
13. Fitz, N. F., Cronican, A. A., Lefterov, I., and Koldamova, R. (2013) Comment on "ApoE-directed therapeutics rapidly clear  $\beta$ -amyloid and reverse deficits in AD mouse models." *Science* **340**, 924
14. Tesseur, I., Lo, A. C., Roberfroid, A., Dietvorst, S., Van Broeck, B., Borgers, M., et al. (2013) Comment on "ApoE-directed therapeutics rapidly clear  $\beta$ -amyloid and reverse deficits in AD mouse models." *Science* **340**, 924
15. Price, A. R., Xu, G., Siemienski, Z. B., Smithson, L. A., Borchelt, D. R., Golde, T. E., et al. (2013) Comment on "ApoE-directed therapeutics rapidly clear  $\beta$ -amyloid and reverse deficits in AD mouse models." *Science* **340**, 924
16. Veeraraghavalu, K., Zhang, C., Miller, S., Hefendehl, J. K., Rajapaksha, T. W., Ulrich, J., et al. (2013) Comment on "ApoE-directed therapeutics rapidly clear  $\beta$ -amyloid and reverse deficits in AD mouse models." *Science* **340**, 924
17. Takasugi, N., Sasaki, T., Suzuki, K., Osawa, S., Isshiki, H., Hori, Y., et al. (2011) BACE1 activity is modulated by cell-associated sphingosine-1-phosphate. *J. Neurosci.* **31**, 6850–6857
18. Alam, S., Afsar, S. Y., Wolter, M. A., Volk, L. M., Mitroi, D. N., Meyer Zu Heringdorf, D., et al. (2023) SIP lyase deficiency in the brain promotes astrogliosis and NLRP3 inflammasome activation via purinergic signaling. *Cells* **12**, 1–20
19. Lei, M., Teo, J. D., Song, H., McEwen, H. P., Yup Lee, J., Couttas, T. A., et al. (2019) Sphingosine kinase 2 potentiates amyloid deposition but protects against hippocampal volume loss and demyelination in a mouse model of Alzheimer's disease. *J. Neurosci.* **39**, 9645–9659
20. Hait, N. C., Maiti, A., Xu, P., Qi, Q., Kawaguchi, T., Okano, M., et al. (2020) Regulation of hypoxia-inducible factor functions in the nucleus by sphingosine-1-phosphate. *FASEB J.* **34**, 4293–4310
21. Lee, Y., Messing, A., Su, M., and Brenner, M. (2008) GFAP promoter elements required for region-specific and astrocyte-specific expression. *Glia* **56**, 481–493
22. Kasahara, Y., Koyama, R., and Ikegaya, Y. (2016) Depth and time-dependent heterogeneity of microglia in mouse hippocampal slice cultures. *Neurosci. Res.* **111**, 64–69
23. Kamikubo, Y., Jin, H., Zhou, Y., Niisato, K., Hashimoto, Y., Takasugi, N., et al. (2023) Ex vivo analysis platforms for monitoring amyloid precursor protein cleavage. *Front. Mol. Neurosci.* **15**, 1068990
24. Kamikubo, Y., Takasugi, N., Niisato, K., Hashimoto, Y., and Sakurai, T. (2017) Consecutive analysis of BACE1 function on developing and developed neuronal cells. *J. Alzheimer's Dis.* **56**, 641–653
25. Laffitte, B. A., Repa, J. J., Joseph, S. B., Wilpitz, D. C., Kast, H. R., Mangelsdorf, D. J., et al. (2001) LXRs control lipid-inducible expression of the apolipoprotein E gene in macrophages and adipocytes. *Proc. Natl. Acad. Sci. U. S. A.* **98**, 507–512
26. Riddell, D. R., Zhou, H., Atchison, K., Warwick, H. K., Atkinson, P. J., Jefferson, J., et al. (2008) Impact of apolipoprotein E (ApoE) polymorphism on brain ApoE levels. *J. Neurosci.* **28**, 11445–11453
27. French, K. J., Zhuang, Y., Maines, L. W., Gao, P., Wang, W., Beljanski, V., et al. (2010) Pharmacology and antitumor activity of ABC294640, a selective inhibitor of sphingosine kinase-2. *J. Pharmacol. Exp. Ther.* **333**, 129–139
28. Kharel, Y., Morris, E. A., Congdon, M. D., Thorpe, S. B., Tomsig, J. L., Santos, W. L., et al. (2015) Sphingosine kinase 2 inhibition and blood sphingosine 1-phosphate levels. *J. Pharmacol. Exp. Ther.* **355**, 23–31
29. Griffin, J. M., Fackelmeier, B., Fong, D. M., Mouravlev, A., Young, D., and O'Carroll, S. J. (2019) Astrocyte-selective AAV gene therapy through the endogenous GFAP promoter results in robust transduction in the rat spinal cord following injury. *Gene Ther.* **26**, 198–210
30. Foo, L. C., Allen, N. J., Bushong, E. A., Ventura, P. B., Chung, W.-S., Zhou, L., et al. (2011) Development of a method for the purification and culture of rodent astrocytes. *Neuron* **71**, 799–811
31. Kihara, A. (2014) Sphingosine 1-phosphate is a key metabolite linking sphingolipids to glycerophospholipids. *Biochim. Biophys. Acta Mol. Cell Biol. Lipids.* **1841**, 766–772
32. Bradley, M. E., McGuinness, N., Williams, G., Charlton, S. J., and Dowling, M. R. (2011) The in vitro metabolism of sphingosine-1-phosphate: identification; inhibition and pharmacological implications. *Eur. J. Pharmacol.* **672**, 56–61
33. Billich, A., Bornancin, F., Dévay, P., Mechtcheriakova, D., Urtz, N., and Baumruker, T. (2003) Phosphorylation of the immunomodulatory drug FTY720 by sphingosine kinases. *J. Biol. Chem.* **278**, 47408–47415
34. Hait, N. C., Allegood, J., Maceyka, M., Strub, G. M., Harikumar, K. B., Singh, S. K., et al. (2009) Regulation of histone acetylation in the nucleus by sphingosine-1-phosphate. *Science* **325**, 1254–1257
35. Hait, N. C., Wise, L. E., Allegood, J. C., O'Brien, M., Avni, D., Reeves, T. M., et al. (2014) Active, phosphorylated fingolimod inhibits histone deacetylases and facilitates fear extinction memory. *Nat. Neurosci.* **17**, 971–980
36. Dominguez, G., Maddelein, M.-L., Pucelle, M., Nicaise, Y., Maurage, C.-A., Duyckaerts, C., et al. (2018) Neuronal sphingosine kinase 2 subcellular localization is altered in Alzheimer's disease brain. *Acta Neuropathol. Commun.* **6**, 25
37. Matsuda, K., Mikami, T., Oki, S., Iida, H., Andrabi, M., Boss, J. M., et al. (2017) ChIP-seq analysis of genomic binding regions of five major transcription factors in mouse epiblast stem cells that highlights a central role for ZIC2. *Development* **144**, 1948–1958
38. Mounier, A., Georgiev, D., Nam, K. N., Fitz, N. F., Castranio, E. L., Wolfe, C. M., et al. (2015) Bexarotene-activated retinoid X receptors regulate neuronal differentiation and dendritic complexity. *J. Neurosci.* **35**, 11862–11876
39. Shi, W.-N., Cui, S.-X., Song, Z.-Y., Wang, S.-Q., Sun, S.-Y., Yu, X.-F., et al. (2017) Overexpression of SphK2 contributes to ATRA resistance in colon cancer through rapid degradation of cytoplasmic RXR $\alpha$  by K48/K63-linked polyubiquitination. *Oncotarget* **8**, 39605–39617
40. Pyne, N. J., Adams, D. R., and Pyne, S. (2017) Sphingosine kinase 2 in autoimmune/inflammatory disease and the development of sphingosine kinase 2 inhibitors. *Trends Pharmacol. Sci.* **38**, 581–591
41. Choi, S., Aljakna, A., Srivastava, U., Peterson, B. R., Deng, B., Prat, A., et al. (2013) Decreased APOE-containing HDL subfractions and cholesterol efflux capacity of serum in mice lacking Pcsk9. *Lipids Health Dis.* **12**, 112
42. Rawat, V., Wang, S., Sima, J., Bar, R., Liraz, O., Gundimeda, U., et al. (2019) ApoE4 alters ABCA1 membrane trafficking in astrocytes. *J. Neurosci.* **39**, 9611–9622
43. Zhang, H., Chen, W., Tan, Z., Zhang, L., Dong, Z., Cui, W., et al. (2020) A role of low-density lipoprotein receptor-related protein 4 (LRP4) in astrocytic A $\beta$  clearance. *J. Neurosci.* **40**, 5347–5361
44. Sato, K., Malchinkhuu, E., Horiuchi, Y., Mogi, C., Tomura, H., Tosaka, M., et al. (2007) Critical role of ABCA1 transporter in sphingosine 1-phosphate release from astrocytes. *J. Neurochem.* **103**, 2610–2619
45. Pérez-Jeldres, T., Alvarez-Lobos, M., and Rivera-Nieves, J. (2021) Targeting sphingosine-1-phosphate signaling in immune-mediated diseases: beyond multiple sclerosis. *Drugs* **81**, 985–1002
46. Lanfranco, M. F., Ng, C. A., and Rebeck, G. W. (2020) ApoE lipidation as a therapeutic target in Alzheimer's disease. *Int. J. Mol. Sci.* **21**, 1–19
47. Lei, M., Shafique, A., Shang, K., Couttas, T. A., Zhao, H., Don, A. S., et al. (2017) Contextual fear conditioning is enhanced in mice lacking functional sphingosine kinase 2. *Behav. Brain Res.* **333**, 9–16
48. Moezzi, S.-M.-I., Mozafari, N., Fazel-Hoseini, S.-M., Nadimi-Parashkoochi, S., Abbasi, H., Ashrafi, H., et al. (2020) Apolipoprotein J

- in Alzheimer's disease: shedding light on its role with cell signaling pathway perspective and possible therapeutic approaches. *ACS Chem. Neurosci.* **11**, 4060–4072
49. Spiegel, S., and Milstien, S. (2011) The outs and the ins of sphingosine-1-phosphate in immunity. *Nat. Rev. Immunol.* **11**, 403–415
  50. Matloubian, M., Lo, C. G., Cinamon, G., Lesneski, M. J., Xu, Y., Brinkmann, V., *et al.* (2004) Lymphocyte egress from thymus and peripheral lymphoid organs is dependent on SIP receptor 1. *Nature.* **427**, 355–360
  51. Takasugi, N., Sasaki, T., Ebinuma, I., Osawa, S., Ishiki, H., Takeo, K., *et al.* (2013) FTY720/fingolimod, a sphingosine analogue, reduces amyloid- $\beta$  production in neurons. *PLoS One* **8**, e64050
  52. Dusaban, S. S., Chun, J., Rosen, H., Purcell, N. H., and Brown, J. H. (2017) Sphingosine 1-phosphate receptor 3 and RhoA signaling mediate inflammatory gene expression in astrocytes. *J. Neuroinflammation.* **14**, 111
  53. Igarashi, N., Okada, T., Hayashi, S., Fujita, T., Jahangeer, S., and Nakamura, S. (2003) Sphingosine kinase 2 is a nuclear protein and inhibits DNA synthesis. *J. Biol. Chem.* **278**, 46832–46839
  54. Ding, G., Sonoda, H., Yu, H., Kajimoto, T., Goparaju, S. K., Jahangeer, S., *et al.* (2007) Protein kinase D-mediated phosphorylation and nuclear export of sphingosine kinase 2. *J. Biol. Chem.* **282**, 27493–27502
  55. Shi, W., Zhang, S., Ma, D., Yan, D., Zhang, G., Cao, Y., *et al.* (2020) Targeting SphK2 reverses acquired resistance of Regorafenib in hepatocellular carcinoma. *Front. Oncol.* **10**, 694
  56. Yang, X., Chen, S., Shao, Z., Li, Y., Wu, H., Li, X., *et al.* (2018) Apolipoprotein E deficiency exacerbates spinal cord injury in mice: inflammatory response and oxidative stress mediated by NF- $\kappa$ B signaling pathway. *Front. Cell. Neurosci.* **12**, 142
  57. Dresselhaus, E., Duerr, J. M., Vincent, F., Sylvain, E. K., Beyna, M., Lanyon, L. F., *et al.* (2018) Class I HDAC inhibition is a novel pathway for regulating astrocytic apoE secretion. *PLoS One.* **13**, e0194661
  58. Dheer, Y., Chitranshi, N., Gupta, V., Abbasi, M., Mirzaei, M., You, Y., *et al.* (2018) Bexarotene modulates retinoid-X-receptor expression and is protective against neurotoxic endoplasmic reticulum stress response and apoptotic pathway activation. *Mol. Neurobiol.* **55**, 9043–9056
  59. Shih, S.-J., Allan, C., Grehan, S., Tse, E., Moran, C., and Taylor, J. M. (2000) Duplicated downstream enhancers control expression of the human apolipoprotein E gene in macrophages and adipose tissue. *J. Biol. Chem.* **275**, 31567–31572
  60. Trusca, V. G., Fuior, E. V., Florea, I. C., Kardassis, D., Simionescu, M., and Gafencu, A. V. (2011) Macrophage-specific up-regulation of apolipoprotein E gene expression by STAT1 is achieved via long range genomic interactions. *J. Biol. Chem.* **286**, 13891–13904
  61. von Eckardstein, A., and Kardassis, D. (2015) High density lipoproteins. In: *Handbook of Experimental Pharmacology*. Springer International Publishing, Cham, Switzerland, 224
  62. Yamashita, S., Masuda, D., and Matsuzawa, Y. (2020) Pemafibrate, a new selective PPAR $\alpha$  modulator: drug concept and its clinical applications for dyslipidemia and metabolic diseases. *Curr. Atheroscler. Rep.* **22**, 5
  63. Parham, K. A., Zebol, J. R., Tooley, K. L., Sun, W. Y., Moldenhauer, L. M., Cockshell, M. P., *et al.* (2015) Sphingosine 1-phosphate is a ligand for peroxisome proliferator-activated receptor- $\gamma$  that regulates neoangiogenesis. *FASEB J.* **29**, 3638–3653
  64. Alam, S., Piazzesi, A., Abd El Fatah, M., Raucamp, M., and van Echten-Deckert, G. (2020) Neurodegeneration caused by S1P-lyase deficiency involves calcium-dependent tau pathology and abnormal histone acetylation. *Cells.* **9**, 2189
  65. Couttas, T. A., Kain, N., Daniels, B., Lim, X. Y., Shepherd, C., Kril, J., *et al.* (2014) Loss of the neuroprotective factor sphingosine 1-phosphate early in Alzheimer's disease pathogenesis. *Acta Neuropathol. Commun.* **2**, 9
  66. He, X., Huang, Y., Li, B., Gong, C.-X., and Schuchman, E. H. (2010) Deregulation of sphingolipid metabolism in Alzheimer's disease. *Neurobiol. Aging.* **31**, 398–408
  67. Okada, T., Ding, G., Sonoda, H., Kajimoto, T., Haga, Y., Khosrowbeygi, A., *et al.* (2005) Involvement of N-terminal-extended form of sphingosine kinase 2 in serum-dependent regulation of cell proliferation and apoptosis. *J. Biol. Chem.* **280**, 36318–36325
  68. Malchinkhuu, E., Sato, K., Muraki, T., Ishikawa, K., Kuwabara, A., and Okajima, F. (2003) Assessment of the role of sphingosine 1-phosphate and its receptors in high-density lipoprotein-induced stimulation of astroglial cell function. *Biochem. J.* **370**, 817–827
  69. Sato, K., Malchinkhuu, E., Horiuchi, Y., Mogi, C., Tomura, H., Tosaka, M., *et al.* (2007) HDL-like lipoproteins in cerebrospinal fluid affect neural cell activity through lipoprotein-associated sphingosine 1-phosphate. *Biochem. Biophys. Res. Commun.* **359**, 649–654
  70. Holtzman, D. M., Herz, J., and Bu, G. (2012) Apolipoprotein E and apolipoprotein E receptors: normal biology and roles in Alzheimer disease. *Cold Spring Harb. Perspect. Med.* **2**, a006312
  71. Cummings, J. L., Zhong, K., Kinney, J. W., Heaney, C., Moll-Tudla, J., Joshi, A., *et al.* (2016) Double-blind, placebo-controlled, proof-of-concept trial of bexarotene in moderate Alzheimer's disease. *Alzheimers. Res. Ther.* **8**, 4
  72. Corder, E. H., Saunders, A. M., Strittmatter, W. J., Schmechel, D. E., Gaskell, P. C., Small, G. W., *et al.* (1993) Gene dose of apolipoprotein E type 4 allele and the risk of Alzheimer's disease in late onset families. *Science* **261**, 921–923
  73. Boehm-Cagan, A., Bar, R., Harats, D., Shaish, A., Levkovitz, H., Bielicki, J. K., *et al.* (2016) Differential effects of apoE4 and activation of ABCA1 on brain and plasma lipoproteins. *PLoS One* **11**, e0166195
  74. Fernández-Calle, R., Konings, S. C., Frontián-Rubio, J., García-Revilla, J., Camprubí-Ferrer, L., Svensson, M., *et al.* (2022) APOE in the bullseye of neurodegenerative diseases: impact of the APOE genotype in Alzheimer's disease pathology and brain diseases. *Mol. Neurodegener.* **17**, 1–47